International Journal of Innovative Computing, Information and Control
Volume **13**, Number **1**, February **2017**

ICIC International ©2017 ISSN 1349-4198
pp. 341–364

PRACTICAL IMPLEMENTATION OF A SIMPLE AND EFFECTIVE ROBUST ADAPTIVE FUZZY VARIABLE STRUCTURE TRAJECTORY TRACKING CONTROL FOR DIFFERENTIAL WHEELED MOBILE ROBOTS

Mauricio Begnini[1], Douglas Wildgrube Bertol[2] and Nardênio Almeida Martins[1,3,*]

[1]Postgraduate Program in Computer Science
Department of Informatics
State University of Maringá
Colombo Avenue, 5790, 87020-900, Maringá, PR, Brazil
pg46937@uem.br; *Corresponding author: namartin@din.uem.br

[2]Group of Systems Automation and Robotics
Department of Electrical Engineering
State University of Santa Catarina
Paulo Malschitzki Street, n/n, 89219-710, Joinville, SC, Brazil
douglas.bertol@udesc.br

[3]Robotics Research Group
Department of Automation and Systems
Federal University of Santa Catarina
Mailbox 476, 88040-900, Florianópolis, SC, Brazil
nardenio@das.ufsc.br

Received June 2016; revised October 2016

Abstract. *In this paper an adaptive fuzzy variable structure control integrated with a proportional-derivative control is proposed as a robust solution to the trajectory tracking control problem for a differential wheeled mobile robot under effect of uncertainties and disturbances. To minimize the problems found in practical implementations of the classical variable structure controllers, a fuzzy logic system replaces the discontinuous portion present in classical forms of the variable structure controllers. This fuzzy logic system does not require an offline tuning process and appears as a feasible tool to approximate any real continuous nonlinear system to arbitrary accuracy. Stability analysis and the convergence of tracking errors are guaranteed with basis on the Lyapunov theory. Simulation and experimental results are explored to verify the effectiveness of the proposed control strategy.*

Keywords: Differential wheeled mobile robot, Trajectory tracking, Adaptive fuzzy variable structure control, Uncertainties and disturbances, Lyapunov theory

1. **Introduction.** An important control problem for the autonomous robot locomotion is the tracking of a given feasible trajectory parameterized in time with robustness despite of uncertainties and disturbances (such as the parametric and structural uncertainties, external disturbances and system limitations) [1-3]. Thus, this paper describes the design of a simple and effective robust kinematic controller, for the differential wheeled mobile robot (DWMR) [4-6], based on the sliding mode theory.

Due to robustness properties against modeling imprecision, uncertainties and disturbances, the variable structure control (VSC) has become very popular and is used in many application areas [7-10]. However, this control scheme has important drawbacks

that limit its practical applicability, such as chattering and large authority control, which deteriorate the system performance [11-14].

Researches have been developed using softcomputing methodologies, such as artificial neural networks and fuzzy logic, in order to improve the performance and reduce the problem found in practical implementations of VSCs [15-17]. In this paper, an adaptive fuzzy variable structure control (AFVSC) is proposed and applied to avoiding the chattering and to compensate the uncertainties and disturbances, since fuzzy logic systems have been proven as a feasible tool to approximate any real continuous nonlinear system to arbitrary accuracy [18].

[19, 20] present adaptive sliding mode controllers for trajectory tracking. The results shown in [19] are presented via simulation in an M shaped trajectory, while [20] presents simulation and experimental results in a straight line trajectory and a circular trajectory. [21] describes a fuzzy sliding mode control, with triangular membership functions where the rules sets use the sliding surfaces and the derivative of the sliding surfaces as input, and the fuzzy output is the gain bounded to the sign function of the sliding mode controller. The results are displayed through simulation in circular trajectory. [22] presented an adaptive fuzzy sliding mode dynamic control with triangular input membership functions and singletons as outputs. The inputs are the sliding surfaces, and the output is a gain to replace the discontinuous function of the sliding mode control. The results are shown via simulation and experimentation with a straight line trajectory and an S shaped trajectory. Also in [23] it presented an fuzzy sliding mode control, with Gaussian membership functions. The inputs are the sliding surfaces and the derivative of the sliding surfaces, and the output is a gain that replaces the discontinuous portion of the sliding mode. The results are presented via simulation in a circular trajectory.

The fuzzy sliding mode control presented in [24, 25] uses triangular membership functions. In [24] it used the tracking errors and the derivative of the tracking errors as fuzzy inputs, and an adjustment of the sliding surface as fuzzy output with an M shaped trajectory, while [25] uses the sliding surface as input, and the output is a gain to replace the value bounded to the sign function in the sliding mode control with a straight line trajectory and an S shaped trajectory.

In [26] the authors show an adaptive fuzzy sliding mode controller, with two fuzzy systems, one with the sliding surfaces and the derivative of the sliding surfaces as input fuzzy sets, and output as a continuous variable to replace the discontinuous portion of the sliding mode control. The second fuzzy system has the errors as input and a normalization factor as output that is bounded to the continuous variable and determines its magnitude. The paper exposes simulations results in a circular trajectory.

The proposed adaptive fuzzy variable structure controller differs from cited works, and others like [27-30] (with simulation results only), in the simplicity and effectiveness of the controller, using only a kinematic variable structure controller, and an adaptive fuzzy system, with reduced number of triangular membership functions (lower computational load), considering only the sliding surface as input and having the output range being updated online.

The following studies [31-47], that consider the kinematics of DWMRs with or without uncertainties and disturbances, also have used the VSC and sliding mode control theories applied in the trajectory tracking control problem of DWMRs, and presented various techniques to eliminate chattering phenomenon. Thus, the differences and contributions of this paper are: development of an AFVSC in Cartesian coordinates, based on the sliding mode theory; development of an adaptive fuzzy system to replace the discontinuous portion of the classical VSC, avoiding the chattering as well as suppressing the uncertainties and disturbances without having any *a priori* knowledge of their limits; stability of

the closed-loop control system with the adaptation law of the fuzzy system are proved using the Lyapunov theory; the integration of the kinematic controller (AFVSC) with a dynamic control (PD or proportional-derivative control) that must ensure a stable and fast tracking of the references despite of neglected dynamics aiming to improve the robustness against chattering; evaluation of the performance of the VSC and AFVSC, by means of simulations and experiments using Matlab/Simulink, MobileSim simulator and the PowerBot DWMR, over a feasible complex eight-shape trajectory; verification that the loss of invariance has little practical meaning [48] and the robustness is ensured in the case of the AFVSC.

This paper is organized as follows. Section 2 presents the kinematic and dynamic models for DWMRs, and the description of the trajectory tracking control problem. The DWMRs kinematic and dynamic controls are summarized in Section 3. In Section 4 the proposed AFVSC, based on the classical VSC, is presented. Section 5 shows the simulation results and experiments in real-time, and Section 6 presents the conclusions.

2. Problem Formulation.

In this section, the kinematic and dynamic models for a DWMR and the control problem to be solved are described.

2.1. Kinematics and dynamics of DWMRs.

A typical example of a DWMR is shown in Figure 1, which is extensively used in literature [47, 49, 50] and correspond to a simple model that represents the main kinematics and dynamics of the DWMR. Disregarding gravitational torques ($\boldsymbol{G}(\boldsymbol{q}) = 0$) and considering uncertainties and disturbances (including external disturbances), the posture dynamic and kinematic models of DWMRs for control purposes are defined as:

$$\dot{\boldsymbol{q}} = \boldsymbol{S}(\boldsymbol{q})\boldsymbol{v}, \tag{1}$$

$$\bar{\boldsymbol{M}}(\boldsymbol{q})\dot{\boldsymbol{v}} + \bar{\boldsymbol{C}}(\boldsymbol{q}, \dot{\boldsymbol{q}})\boldsymbol{v} + \boldsymbol{\delta}(\boldsymbol{q}, \boldsymbol{v}) = \bar{\boldsymbol{D}}(\boldsymbol{q})\boldsymbol{\tau}, \tag{2}$$

where $\boldsymbol{q}$ is the posture vector in the plane, $\boldsymbol{v} = [\upsilon\ \omega]^{\mathrm{T}}$ is the velocity vector, with longitudinal velocity (υ), and rotational velocity (ω), $\boldsymbol{\tau}$ is the torque vector, $\bar{\boldsymbol{M}}(\boldsymbol{q}) = \boldsymbol{S}^{\mathrm{T}}(\boldsymbol{q})\boldsymbol{M}(\boldsymbol{q})\boldsymbol{S}(\boldsymbol{q})$, $\bar{\boldsymbol{C}}(\boldsymbol{q}, \dot{\boldsymbol{q}}) = \boldsymbol{S}^{\mathrm{T}}(\boldsymbol{q})\boldsymbol{M}(\boldsymbol{q})\dot{\boldsymbol{S}}(\boldsymbol{q}, \dot{\boldsymbol{q}}) + \boldsymbol{S}^{\mathrm{T}}(\boldsymbol{q})\boldsymbol{C}(\boldsymbol{q}, \dot{\boldsymbol{q}})\boldsymbol{S}(\boldsymbol{q})$, $\bar{\boldsymbol{D}}(\boldsymbol{q}) = \boldsymbol{S}^{\mathrm{T}}(\boldsymbol{q})\boldsymbol{D}(\boldsymbol{q})$ [47, 49, 50], and

$$\boldsymbol{\delta}(\boldsymbol{q}, \boldsymbol{v}) = \Delta\bar{\boldsymbol{M}}(\boldsymbol{q})\dot{\boldsymbol{v}} + \Delta\bar{\boldsymbol{C}}(\boldsymbol{q}, \dot{\boldsymbol{q}})\boldsymbol{v} + \bar{\boldsymbol{\tau}}_{\mathrm{p}}, \tag{3}$$

being that $\Delta\bar{\boldsymbol{M}}(\boldsymbol{q})$ and $\Delta\bar{\boldsymbol{C}}(\boldsymbol{q}, \dot{\boldsymbol{q}})$ denote unknown internal uncertainties, including both parametric and nonparametric uncertainties, and $\bar{\boldsymbol{\tau}}_{\mathrm{p}} = \boldsymbol{S}^{\mathrm{T}}(\boldsymbol{q})\boldsymbol{\tau}_{\mathrm{p}}$ denotes uncertainties and disturbances (e.g., nonparametric uncertainties and external disturbances) [49]. The Jacobian matrix $\boldsymbol{S}(\boldsymbol{q})$, the nominal inertia matrix $\boldsymbol{M}(\boldsymbol{q})$, the Coriolis and centrifugal matrix $\boldsymbol{C}(\boldsymbol{q}, \dot{\boldsymbol{q}})$, and the input transformation matrix $\boldsymbol{D}(\boldsymbol{q})$ are provided in [50], which are representative of the PowerBot DWMR and are used for simulation of the proposed controllers.

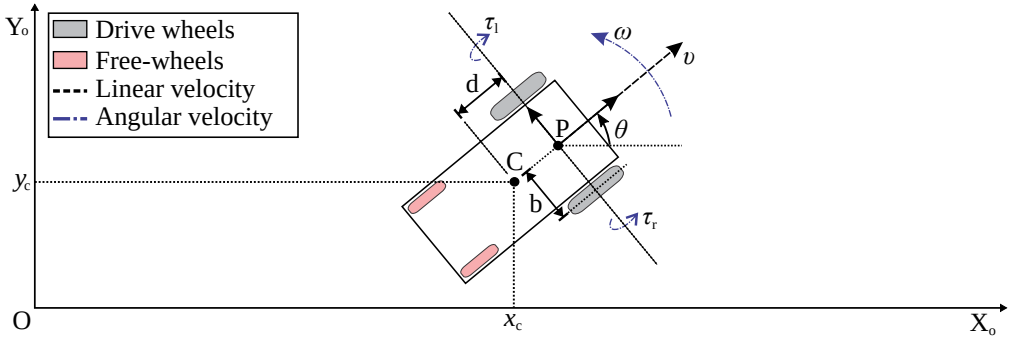

FIGURE 1. DWMR and coordinate systems

2.2. **Problem statement.** The trajectory tracking control problem for DWMRs [51] is accomplished by proposing a control structure that uses adaptive and fuzzy controls based on VSC (i.e., AFVSC) for the design of a robust kinematic controller that avoids chattering and makes the posture tracking errors (or posture error) tend to zero quickly, and an dynamic control with a PD for the design of a dynamic controller that makes the auxiliary velocity tracking errors also tend to zero quickly.

3. **Control Project.** Let the control synthesis be treated separately by presenting first the dynamic control design and then the kinematic control design.

3.1. **Dynamic control.** The objective of the dynamic controller is to ensure fast auxiliary velocity tracking errors $\boldsymbol{v}_{\mathrm{e}} = \boldsymbol{v}_{\mathrm{c}} - \boldsymbol{v}$. As the uncertainties $\boldsymbol{\psi}$ are unknown, they are set to zero for the purpose of this design and will be considered just for adjusting control gain and the design of the kinematic controller.

To act as the dynamic controller, it is considered of the solution presented by [52, Chapter 8] about the calculus of the PD control. So it has to change the applied wheels torque control to the body torques:

$$\boldsymbol{\tau} = \bar{\boldsymbol{D}}(\boldsymbol{q})^{-1}\,\bar{\boldsymbol{u}}, \tag{4}$$

and apply to the system, Equation (2), the control law $\bar{\boldsymbol{u}} = [\bar{u}_{\upsilon}\ \bar{u}_{\omega}]^{\mathrm{T}}$ as a new control input that will be designed as PD control to achieve fast convergence of $\boldsymbol{v}_{\mathrm{e}}$. Thus, the control signals $\bar{u}_{\upsilon}(s)$ and $\bar{u}_{\omega}(s)$ [50] are generated by the PD controller as follows:

$$C_{\upsilon}(s) = \frac{\upsilon(s)}{\bar{u}_{\upsilon}(s)} = \mathrm{k}_{\mathrm{p}\upsilon} + \frac{\mathrm{k}_{\mathrm{d}\upsilon}\eta_{\upsilon}}{1 + \frac{\eta_{\upsilon}}{s}}, \quad C_{\omega}(s) = \frac{\omega(s)}{\bar{u}_{\omega}(s)} = \mathrm{k}_{\mathrm{p}\omega} + \frac{\mathrm{k}_{\mathrm{d}\omega}\eta_{\omega}}{1 + \frac{\eta_{\omega}}{s}}, \tag{5}$$

with the proportional gains, $\mathrm{k}_{\mathrm{p}\upsilon}$ and $\mathrm{k}_{\mathrm{p}\omega}$, the derivative gains, $\mathrm{k}_{\mathrm{d}\upsilon}$ and $\mathrm{k}_{\mathrm{d}\omega}$, and the derivative filter parameter gains η_{υ} and η_{ω} being positive and adjusted to achieve stability with good time response performance. The adjustment of η_{υ} and η_{ω} plays an important role in accelerating the system response in spite of the neglected dynamics and to avoid excitation as well as the chattering phenomenon [50].

This dynamic control architecture ensures fast auxiliary velocity tracking errors, as seen in [52] and is proved asymptotically stable by Lyapunov theory considering the reference velocity constant. However, in this work, the reference velocity is time-varying, which violates the stability proof losing its asymptotic characteristic. So this residual error will be handled by the VSC at the kinematic control.

Further, the authors of this work are aware that the VSC could handle the entire control problem without the PD controller, but as the real DWMR that is used as experimental platform (the PowerBot DWMR) has in its firmware this PD controller as a basic and unremovable dynamic control in the architecture (the DWMR cannot be directly torque controlled), it has to reflect this architecture in the simulations and to the entire solution.

3.2. **Kinematic control.** To design a kinematic controller, capable of calculating the inputs υ and ω, to solve the trajectory tracking control problem, a reference trajectory generated by a virtual DWMR is needed. The kinematics of the virtual DWMR is modeled as:

$$\dot{\boldsymbol{q}}_{\mathrm{r}} = \boldsymbol{S}(\boldsymbol{q}_{\mathrm{r}})\boldsymbol{v}_{\mathrm{r}}, \quad \dot{x}_{\mathrm{r}} = \upsilon_{\mathrm{r}}\cos\theta_{\mathrm{r}}, \quad \dot{y}_{\mathrm{r}} = \upsilon_{\mathrm{r}}\sin\theta_{\mathrm{r}}, \quad \dot{\theta}_{\mathrm{r}} = \omega_{\mathrm{r}}, \tag{6}$$

where $\boldsymbol{q}_{\mathrm{r}} = [x_{\mathrm{r}}\ y_{\mathrm{r}}\ \theta_{\mathrm{r}}]^{\mathrm{T}}$ is the reference posture vector of the virtual DWMR, and $\boldsymbol{v}_{\mathrm{r}} = [\upsilon_{\mathrm{r}}\ \omega_{\mathrm{r}}]^{\mathrm{T}}$ is the reference velocity vector of the virtual DWMR.

Converting the posture tracking errors in the inertial frame to the DWMR frame, the posture error equation of the DWMR can be denoted as [53]:

$$\boldsymbol{q}_{\mathrm{e}} = \begin{bmatrix} x_{\mathrm{e}} \\ y_{\mathrm{e}} \\ \theta_{\mathrm{e}} \end{bmatrix} = \begin{bmatrix} \cos\theta & \sin\theta & 0 \\ -\sin\theta & \cos\theta & 0 \\ 0 & 0 & 1 \end{bmatrix} \begin{bmatrix} x_{\mathrm{r}} - x_{\mathrm{c}} \\ y_{\mathrm{r}} - y_{\mathrm{c}} \\ \theta_{\mathrm{r}} - \theta \end{bmatrix}, \tag{7}$$

consequently the error dynamics of the closed-loop system for trajectory tracking is obtained from the time derivative of Equation (7), after mathematical manipulations, as:

$$\begin{cases} \dot{x}_{\mathrm{e}} = \omega y_{\mathrm{e}} - \upsilon + \upsilon_{\mathrm{r}} \cos\theta_{\mathrm{e}} \\ \dot{y}_{\mathrm{e}} = -\omega x_{\mathrm{e}} + \upsilon_{\mathrm{r}} \sin\theta_{\mathrm{e}} \\ \dot{\theta}_{\mathrm{e}} = \omega_{\mathrm{r}} - \omega \end{cases}. \tag{8}$$

Under robustness considerations, in practical situations, the velocities and tracking errors are not equal to zero [51]. As perfect velocity tracking does not hold in practice, the dynamic controller generates auxiliary velocity tracking errors $\boldsymbol{v}_{\mathrm{e}}$, which is bounded by some known constants. This tracking error can be seen as an uncertainty and disturbance for the kinematic model, see Figure 2, that satisfies the matching condition, i.e., the nonholonomic constraint $\dot{y}_{\mathrm{c}} \cos\theta - \dot{x}_{\mathrm{c}} \sin\theta = 0$ is not violated. This will be seen in the results obtained by simulations and experiments, thereby determining the robustness of the proposed kinematic controller. To design the proposed kinematic controller, which is based on VSC theory, it is required of the selection of the sliding surfaces and a brief description of the generic modeling of nonlinear systems to the VSC design [7, 8, 10].

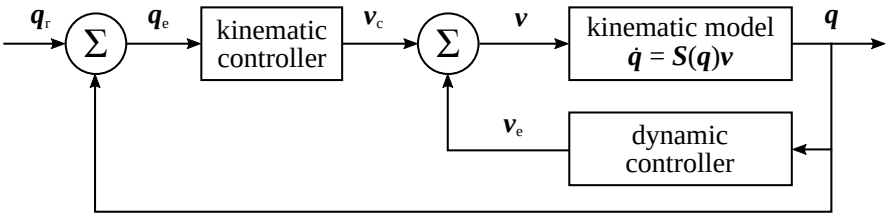

FIGURE 2. Block diagram of the closed-loop control system: $\boldsymbol{v}_{\mathrm{e}}$ as uncertainty and disturbance for the kinematic model (similar to [51])

3.2.1. *Sliding surfaces.* The VSC is a feedback control with high-speed switching, whose action is divided in two phases: the reaching phase and the sliding phase. In the reaching phase, the state trajectories of the system are lead to a place in the state space chosen by the designer. In general, this place is defined by linear surfaces of the control errors ($\tilde{\boldsymbol{z}} = \boldsymbol{q}_{\mathrm{e}} = [x_{\mathrm{e}}\ y_{\mathrm{e}}\ \theta_{\mathrm{e}}]^{\mathrm{T}}$), known as sliding surfaces ($\boldsymbol{\sigma}$), which are described by:

$$\boldsymbol{\sigma}(\tilde{\boldsymbol{z}}, t) = \boldsymbol{\Lambda}^{\mathrm{T}} \tilde{\boldsymbol{z}} = 0. \tag{9}$$

In the sliding phase, the state trajectories are forced to remain on the sliding surfaces. Therefore, during this phase, the errors tend exponentially to zero according to a standard determined by a matrix of positive constants $\boldsymbol{\Lambda}^{\mathrm{T}}$ of Equation (9), which is chosen by the designer.

Thus, from the error dynamics Equation (8), the following sliding surfaces are selected:

$$\boldsymbol{\sigma}(\tilde{\boldsymbol{z}}, t) = \begin{bmatrix} \sigma_1 \\ \sigma_2 \end{bmatrix} = \begin{bmatrix} \Lambda_1 x_{\mathrm{e}} \\ \Lambda_2 y_{\mathrm{e}} + \Lambda_3 \theta_{\mathrm{e}} \end{bmatrix}, \tag{10}$$

where Λ_1, Λ_2, Λ_3 are positive constants.

It should be emphasized that the selection of the sliding surfaces is a critical and difficult problem for the VSC design due to the fact that the posture error Equation (7), represents a nonlinear system of multiple inputs [41].

3.2.2. *Generic model for nonlinear systems.* The generic model is obtained from the derivation of VSC and their properties obtained directly for a class of nonlinear systems, i.e.,

$$\dot{\tilde{\boldsymbol{z}}} = \boldsymbol{A}(\tilde{\boldsymbol{z}}, \boldsymbol{p}, t) + \boldsymbol{B}(\tilde{\boldsymbol{z}}, \boldsymbol{p}, t)\boldsymbol{v}(\tilde{\boldsymbol{z}}, t) + \boldsymbol{d}_{\mathrm{b}}(t), \tag{11}$$

being that $\boldsymbol{A}(\tilde{\boldsymbol{z}}, \boldsymbol{p}, t) = \boldsymbol{A}_0(\tilde{\boldsymbol{z}}, t) + \Delta\boldsymbol{A}(\tilde{\boldsymbol{z}}, \boldsymbol{p}, t)$, $\boldsymbol{B}(\tilde{\boldsymbol{z}}, \boldsymbol{p}, t) = \boldsymbol{B}_0(\tilde{\boldsymbol{z}}, t) + \Delta\boldsymbol{B}(\tilde{\boldsymbol{z}}, \boldsymbol{p}, t)$, $\boldsymbol{d}_{\mathrm{b}}(t) = \boldsymbol{B}_0(\tilde{\boldsymbol{z}}, t)\tilde{\boldsymbol{d}}_0$, and further information can be found in [10, 47]. Such generic model must present robustness to uncertainties and disturbances in the kinematic model Equation (1). To ensure the robustness of the controller, the uncertainties and disturbances must be bounded, the matrix $\boldsymbol{B}(\tilde{\boldsymbol{z}}, t)$ must be nonsingular, and conditions must be satisfied [10,47]. With basis in this control theory, the error dynamics in Equation (8) can be written as:

$$\dot{\tilde{\boldsymbol{z}}} = \boldsymbol{A}_0(\tilde{\boldsymbol{z}}, t) + \boldsymbol{B}_0(\tilde{\boldsymbol{z}}, t)\boldsymbol{v}(\tilde{\boldsymbol{z}}, t) + \boldsymbol{d}_{\mathrm{b}}(t) \tag{12}$$

since there are no parametric uncertainties ($\Delta\boldsymbol{A} = 0$, $\Delta\boldsymbol{B} = 0$).

3.2.3. *Controller design.* In order to influence also on the process of reaching the sliding surfaces, the control $\boldsymbol{v}(\tilde{\boldsymbol{z}}, t)$ will be chosen in such a way to impose $\boldsymbol{\sigma}(\tilde{\boldsymbol{z}}, t)$ to have the dynamics given by the following first order differential equation:

$$\dot{\boldsymbol{\sigma}}(\tilde{\boldsymbol{z}}, t) = -\mathbf{G}\, sign(\boldsymbol{\sigma}) - \mathbf{K}\, h(\boldsymbol{\sigma}), \tag{13}$$

where $\mathbf{G} = diag[\mathrm{g}_1 \ldots \mathrm{g}_n \ldots \mathrm{g}_{\mathrm{N}}]$ and $\mathbf{K} = diag[\kappa_1 \ldots \kappa_n \ldots \kappa_{\mathrm{N}}]$ are positive definite diagonal matrices, $sign(\boldsymbol{\sigma}) = \frac{\boldsymbol{\sigma}}{|\boldsymbol{\sigma}|}$ is a discontinuous function, and $h(\boldsymbol{\sigma}) = \boldsymbol{\sigma}$ (could be another function, since $\boldsymbol{\sigma}^{\mathrm{T}} h(\boldsymbol{\sigma}) > 0$).

Using Equation (9), Equation (12) and Equation (13) results in:

$$\dot{\boldsymbol{\sigma}}(\tilde{\boldsymbol{z}}, t) = \frac{\partial\boldsymbol{\sigma}(\tilde{\boldsymbol{z}}, t)}{\partial\tilde{\boldsymbol{z}}}\dot{\tilde{\boldsymbol{z}}} + \frac{\partial\boldsymbol{\sigma}(\tilde{\boldsymbol{z}}, t)}{\partial t} = \frac{\partial\boldsymbol{\sigma}}{\partial\tilde{\boldsymbol{z}}}(\boldsymbol{A}_0 + \boldsymbol{B}_0\boldsymbol{v}) + \frac{\partial\boldsymbol{\sigma}}{\partial\tilde{\boldsymbol{z}}}\boldsymbol{d}_{\mathrm{b}} + \frac{\partial\boldsymbol{\sigma}}{\partial t} = -\mathbf{G}\, sign(\boldsymbol{\sigma}) - \mathbf{K}\boldsymbol{\sigma} \tag{14}$$

with

$$\frac{\partial\boldsymbol{\sigma}(\tilde{\boldsymbol{z}}, t)}{\partial t} = 0, \quad \frac{\partial\boldsymbol{\sigma}(\tilde{\boldsymbol{z}}, t)}{\partial\tilde{\boldsymbol{z}}} = \boldsymbol{\Lambda}^{\mathrm{T}} = \begin{bmatrix} \Lambda_1 & 0 & 0 \\ 0 & \Lambda_2 & \Lambda_3 \end{bmatrix},$$

whence is derived the following control law:

$$\boldsymbol{v} = -\boldsymbol{B}_{0\sigma}^{-1}\left(\boldsymbol{A}_{0\sigma} + \mathbf{G}\, sign(\boldsymbol{\sigma}) + \mathbf{K}\boldsymbol{\sigma}\right), \tag{15}$$

in which

$$\boldsymbol{A}_{0\sigma} = \frac{\partial\boldsymbol{\sigma}}{\partial\tilde{\boldsymbol{z}}}\boldsymbol{A}_0 = \begin{bmatrix} \Lambda_1 \upsilon_{\mathrm{r}} \cos(\theta_{\mathrm{e}}) \\ \Lambda_2 \upsilon_{\mathrm{r}} \sin(\theta_{\mathrm{e}}) + \Lambda_3 \omega_{\mathrm{r}} \end{bmatrix}, \tag{16}$$

$$\boldsymbol{B}_{0\sigma} = \frac{\partial\boldsymbol{\sigma}}{\partial\tilde{\boldsymbol{z}}}\boldsymbol{B}_0 = \begin{bmatrix} -\Lambda_1 & \Lambda_1 y_{\mathrm{e}} \\ 0 & -\Lambda_2 x_{\mathrm{e}} - \Lambda_3 \end{bmatrix}, \tag{17}$$

$$\boldsymbol{B}_{0\sigma}^{-1} = \begin{bmatrix} -\dfrac{1}{\Lambda_1} & -\dfrac{y_{\mathrm{e}}}{\Lambda_2 x_{\mathrm{e}} + \Lambda_3} \\ 0 & -\dfrac{1}{\Lambda_2 x_{\mathrm{e}} + \Lambda_3} \end{bmatrix}. \tag{18}$$

Replacing Equation (15) in Equation (14) results in:

$$\dot{\boldsymbol{\sigma}} = \boldsymbol{A}_{0\sigma} - \boldsymbol{B}_{0\sigma}\boldsymbol{B}_{0\sigma}^{-1}\left(\boldsymbol{A}_{0\sigma} + \mathbf{G}\, sign(\boldsymbol{\sigma}) + \mathbf{K}\boldsymbol{\sigma}\right) + \boldsymbol{d}_{\sigma} = -\mathbf{G}\, sign(\boldsymbol{\sigma}) - \mathbf{K}\boldsymbol{\sigma} + \boldsymbol{d}_{\sigma} \tag{19}$$

where $\boldsymbol{B}_{0\sigma}\boldsymbol{B}_{0\sigma}^{-1} = \mathbf{I}_{\mathrm{n}}$, and $\boldsymbol{d}_{\sigma} = \frac{\partial\boldsymbol{\sigma}}{\partial\tilde{\boldsymbol{z}}}\boldsymbol{d}_{\mathrm{b}}$ are the uncertainties and disturbances in the system.

3.2.4. *Stability analysis.* Choosing the Lyapunov function candidate in the form:

$$V = \frac{1}{2}\boldsymbol{\sigma}^{\mathrm{T}}\boldsymbol{\sigma} \tag{20}$$

which is positive definite, the sliding surface will be attractive since that the control law Equation (15), ensures that $\dot{V} = \boldsymbol{\sigma}^{\mathrm{T}}\dot{\boldsymbol{\sigma}}$ is negative definite. Using the result described by Equation (19), $\dot{V}$ is immediately obtained as:

$$\dot{V} = \boldsymbol{\sigma}^{\mathrm{T}}\dot{\boldsymbol{\sigma}} = -\boldsymbol{\sigma}^{\mathrm{T}}\mathbf{G}\, sign(\boldsymbol{\sigma}) - \boldsymbol{\sigma}^{\mathrm{T}}\mathbf{K}\boldsymbol{\sigma} + \boldsymbol{\sigma}^{\mathrm{T}}\boldsymbol{d}_{\sigma}. \tag{21}$$

As $\boldsymbol{\sigma}^{\mathrm{T}}\mathbf{K}\boldsymbol{\sigma} \geq 0$, the condition $\dot{V} \leq 0$ can be expressed by:

$$\boldsymbol{\sigma}^{\mathrm{T}}\mathbf{G}\, sign(\boldsymbol{\sigma}) \geq \boldsymbol{\sigma}^{\mathrm{T}}\boldsymbol{d}_{\sigma}, \tag{22}$$

which is satisfied if the diagonal elements of $\mathbf{G}$ meet the following constraint:

$$\mathrm{g}_n > |\boldsymbol{d}_{\sigma}|, \quad n = 1, \ldots, \mathrm{N} \tag{23}$$

where g_n is minimum singular value of $\mathbf{G}$ and $|\boldsymbol{d}_{\sigma}|$ is the maximum effect of the uncertainties and/or disturbances. If $\mathrm{g}_n > |\boldsymbol{d}_{\sigma}|$, then $\dot{V} \leq 0$ ($\dot{V} = 0$ only when $V = 0$), which implies that V may decrease to $V = 0$ exponentially; however, if $\mathrm{g}_n < |\boldsymbol{d}_{\sigma}|$ there is a value of $V = V_{\mathrm{ss}} > 0$ for which $\dot{V} = 0$ can lead to nonzero errors. Therefore, it is possible to affirm that if the uncertainties and disturbances are better estimated, the results will be better.

To the existence and reachability of a sliding mode, the Lyapunov function candidate must be positive, so that the sliding surface will be attractive if the control law Equation (15), ensures $\dot{V} \leq 0$. Then, a nonsingular matrix $\boldsymbol{B}_{0\sigma}$ is necessary. As $\mathbf{G}$, in Equation (15) is a positive definite diagonal matrix, the sliding mode can be forced to the condition where the matrix $\boldsymbol{B}_{0\sigma}$ is also positive definite, and the values of $\mathbf{G}$ are large enough. However, in Equation (15) the matrix $\boldsymbol{B}_{0\sigma}$ is only nonsingular. To solve this problem, a method of diagonalization was used, requiring new sliding surfaces $\boldsymbol{\sigma}^*(\tilde{\boldsymbol{z}}, t)$ [44]:

$$\boldsymbol{\sigma}^*(\tilde{\boldsymbol{z}}, t) = \boldsymbol{\Gamma}(\tilde{\boldsymbol{z}}, t)\boldsymbol{\sigma}(\tilde{\boldsymbol{z}}, t) = \boldsymbol{\Gamma}(\tilde{\boldsymbol{z}}, t)\boldsymbol{\Lambda}^{\mathrm{T}}\tilde{\boldsymbol{z}}, \tag{24}$$

where $\boldsymbol{\Gamma}(\tilde{\boldsymbol{z}}, t) \in \Re^{\mathrm{n}\times\mathrm{n}}$ is a suitable nonsingular transformation. This method is based on the fact that the equivalent system is invariant to a nonsingular transformation of the sliding surfaces [54]. The suitable nonsingular transformation $\boldsymbol{\Gamma}(\tilde{\boldsymbol{z}}, t)$ is defined as [44]:

$$\boldsymbol{\Gamma}(\tilde{\boldsymbol{z}}, t) = \left(\frac{\partial\boldsymbol{\sigma}}{\partial\tilde{\boldsymbol{z}}}\boldsymbol{B}_0\right)^{\mathrm{T}} = \boldsymbol{B}_{0\sigma}^{\mathrm{T}}. \tag{25}$$

With the new sliding surfaces, considering Equations (14), (16), (17), (18), (20) and after mathematical manipulations, $\dot{V}$ is obtained as:

$$\dot{V} = -\boldsymbol{\sigma}^{\mathrm{T}}\dot{\boldsymbol{\sigma}} = \boldsymbol{\sigma}^{*^{\mathrm{T}}}\boldsymbol{B}_{0\sigma}^{-1}\boldsymbol{A}_{0\sigma} + \boldsymbol{\sigma}^{*^{\mathrm{T}}}\left(\boldsymbol{v} + \tilde{\boldsymbol{d}}_0\right). \tag{26}$$

Selecting control law $\boldsymbol{v}$ as:

$$\boldsymbol{v} = -\boldsymbol{B}_{0\sigma}^{-1}\boldsymbol{A}_{0\sigma} - \mathbf{G}\, sign(\boldsymbol{\sigma}^*) - \mathbf{K}\boldsymbol{\sigma}^*, \tag{27}$$

and replacing Equation (27) into Equation (26), $\dot{V}$ is rewritten as:

$$\dot{V} = -\boldsymbol{\sigma}^{*^{\mathrm{T}}}\mathbf{G}\, sign(\boldsymbol{\sigma}^*) - \boldsymbol{\sigma}^{*^{\mathrm{T}}}\mathbf{K}\boldsymbol{\sigma}^* + \boldsymbol{\sigma}^{*^{\mathrm{T}}}\tilde{\boldsymbol{d}}_0. \tag{28}$$

As Equation (28) is similar to Equation (21), the same conclusion about the stability may be taken. Moreover, sliding mode occurs in the manifold $\boldsymbol{\sigma}^*(\tilde{\boldsymbol{z}}, t) = 0$. The transformation in Equation (24) and Equation (25) is nonsingular, therefore, the manifolds $\boldsymbol{\sigma}(\tilde{\boldsymbol{z}}, t) = 0$ and $\boldsymbol{\sigma}^*(\tilde{\boldsymbol{z}}, t) = 0$ coincide and sliding mode takes place in the manifold $\boldsymbol{\sigma}(\tilde{\boldsymbol{z}}, t) = 0$, which was selected to design sliding motion with the desired properties.

4. **Control Design Considering Chattering Attenuation.** Unfortunately, in practical implementation, due to delays, neglected dynamics, sampling frequency limitation, physical limitations of actuators and imperfections of switching, it is not possible to switch the control from a value to another instantaneously [44, 50]. Thus, the state trajectory varies in a vicinity around the sliding surface, instead of sliding over it. This phenomenon, known as chattering, can be avoided or at least reduced replacing the discontinuous function $sign(\boldsymbol{\sigma}^*)$ by a continuous approximation.

Such approximation can avoid chattering but the invariance principle is not verified anymore, theoretically reducing the robustness (such reduction is not significant and the robustness is ensured). However, the smooth control signal is achieved [44, 47]. This occurs because the system dynamics in this case is conned to a neighborhood of the sliding surfaces, and no longer over it, i.e., as a consequence of the approximation the system is enforced to a neighborhood of the manifolds $\boldsymbol{\sigma}(\tilde{\boldsymbol{z}}, t) = 0$ and $\boldsymbol{\sigma}^*(\tilde{\boldsymbol{z}}, t) = 0$ resulting in a reduction of the original robustness that can be acceptable. Moreover, realization of the invariance requires that switching between the reaching phase and the sliding phase is ideal, which is impractical. Therefore, the invariance is ideal and has little practical meaning [48]. Another problem with VSC is the need of knowledge of the limits of uncertainties and disturbances in the system, and the application of a large value to the gains $\mathbf{G}$ that can cause a high control effort (large authority control), affecting the trajectory tracking and deteriorating the system performance [44].

In order to get better results without the need of the knowledge of the limits of uncertainties and disturbances in the system, in this section an AFVSC is proposed to deal with the chattering.

4.1. **Introducing fuzzy systems.** As shown in the block diagram of Figure 3, a fuzzy system has four basic parts: fuzzification, fuzzy rule base, inference machine, and defuzzification. Given a set of non-fuzzy entry, from an external system, the fuzzification is responsible for mapping these entries to input fuzzy sets. The fuzzy rule base represents knowledge in the form of linguistic sentences. The rules are written in the form "if ... then ..." describing a relation between the input space and the output space. Then, for each rule, the inference machine maps an input set to an output fuzzy set, according to the relation defined by the rules, combining the fuzzy sets from all the rules in the rule base into the output fuzzy set. Finally, the defuzzification translates fuzzy output to a real number for the system. All the four parts can be mathematically formulated. Further details can be found in [18, 55].

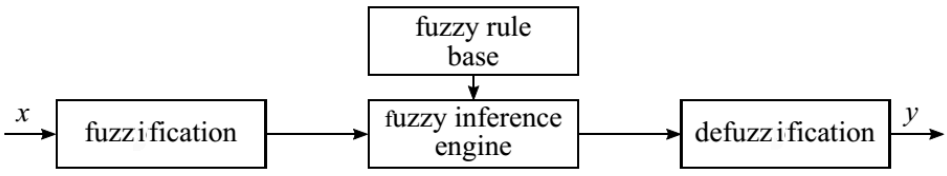

FIGURE 3. Representation in block diagram of a fuzzy system

In this paper, the output y of a single-input single-output (SISO) fuzzy system with M rules considering the input x can be written as:

$$y = \frac{\sum_{m=1}^{\mathrm{M}} \beta^m \mu^m(x)}{\sum_{m=1}^{\mathrm{M}} \mu^m(x)} = \boldsymbol{\beta}^{\mathrm{T}} \boldsymbol{\psi}(x), \tag{29}$$

where $\boldsymbol{\beta} = \left[\beta^1 \dots \beta^m \dots \beta^{\mathrm{M}}\right]^{\mathrm{T}}$ is the vector of consequences, $\boldsymbol{\psi}(x) = \left[\psi^1(x) \dots \psi^m(x) \dots \psi^{\mathrm{M}}(x)\right]^{\mathrm{T}}$ is the vector of weights in which

$$\psi^m(x) = \frac{\mu^m(x)}{\sum\limits_{m=1}^{\mathrm{M}} \mu^m(x)},$$

with $\mu^m(x)$ being the membership function of the input x in the rule m.

4.2. **Design of the adaptive fuzzy variable structure control (AFVSC).** The chattering in the control law presented in Equation (27) is caused by the constant value of $\mathbf{G}$ and the discontinuous function $sign(\boldsymbol{\sigma}^*)$. Let the control gain $\mathbf{G}\, sign(\boldsymbol{\sigma}^*)$ be replaced by a fuzzy system $\hat{\boldsymbol{F}}(\boldsymbol{\sigma}^*)$. The new control input (AFVSC) is then written as:

$$\boldsymbol{v} = -\boldsymbol{B}_{0\sigma}^{-1}\boldsymbol{A}_{0\sigma} - \hat{\boldsymbol{F}}(\boldsymbol{\sigma}^*) - \mathbf{K}\boldsymbol{\sigma}^*, \tag{30}$$

where the fuzzy system is defined as $\hat{\boldsymbol{F}}\left(\boldsymbol{\sigma}^*\right) = \left[\hat{f}_1(\sigma_1^*) \dots \hat{f}_n(\sigma_n^*) \dots \hat{f}_{\mathrm{N}}(\sigma_{\mathrm{N}}^*)\right]^{\mathrm{T}}$ and each $\hat{f}_n(\sigma_n^*)$ is estimated by an individual fuzzy system that can be written as:

$$\hat{f}_n(\sigma_n^*) = \frac{\sum\limits_{m=1}^{\mathrm{M}} \hat{\boldsymbol{\beta}}_n^m \mu_n^m(\sigma_n^*)}{\sum\limits_{m=1}^{\mathrm{M}} \mu_n^m(\sigma_n^*)} = \hat{\boldsymbol{\beta}}_n^{\mathrm{T}} \boldsymbol{\psi}_n(\sigma_n^*) \tag{31}$$

where $\hat{\boldsymbol{\beta}}_n = \left[\hat{\beta}_n^1 \dots \hat{\beta}_n^m \dots \hat{\beta}_n^{\mathrm{M}}\right]^{\mathrm{T}}$ is the vector of consequences, and $\boldsymbol{\psi}_n(\sigma_n^*) = \left[\psi_n^1(\sigma_n^*) \dots \psi_n^m(\sigma_n^*) \dots \psi_n^{\mathrm{M}}(\sigma_n^*)\right]^{\mathrm{T}}$ is the vector of weights. For the purpose of an online update of the parameters of $\hat{f}_n(\sigma_n^*)$, the consequences $\hat{\boldsymbol{\beta}}_n$ are chosen as the parameters to be updated.

Define $\boldsymbol{\beta}_n$, so that $f(\sigma_n^*)_n = \boldsymbol{\beta}_n^{\mathrm{T}} \boldsymbol{\psi}_n(\sigma_n^*)$ is the optimal compensation for $\tilde{\boldsymbol{d}}_{0_n}$. According to Wang's theorem [18, 55] there exists $\gamma_n > 0$, satisfying

$$\left|\tilde{\boldsymbol{d}}_{0_n} - \boldsymbol{\beta}_n^{\mathrm{T}} \boldsymbol{\psi}_n(\sigma_n^*)\right| \leq \gamma_n, \tag{32}$$

where γ_n can be as small as possible, i.e., $0 < \gamma_n < 1$. Now define the estimation error as

$$\tilde{\boldsymbol{\beta}}_n = \hat{\boldsymbol{\beta}}_n - \boldsymbol{\beta}_n, \tag{33}$$

so Equation (31) can be rewritten as

$$\hat{f}_n(\sigma_n^*) = \tilde{\boldsymbol{\beta}}_n^{\mathrm{T}} \boldsymbol{\psi}_n(\sigma_n^*) + \boldsymbol{\beta}_n^{\mathrm{T}} \boldsymbol{\psi}_n(\sigma_n^*), \tag{34}$$

and the adaptive law can be chosen as

$$\dot{\tilde{\boldsymbol{\beta}}}_n = \dot{\hat{\boldsymbol{\beta}}}_n = \sigma_n^* \boldsymbol{\psi}_n(\sigma_n^*). \tag{35}$$

4.3. **Stability analysis of the AFVSC.** Let the Lyapunov function candidate be:

$$V = \frac{1}{2}\left[\boldsymbol{\sigma}^{\mathrm{T}}\boldsymbol{\sigma} + \sum_{n=1}^{\mathrm{N}} \left(\tilde{\boldsymbol{\beta}}_n^{\mathrm{T}} \tilde{\boldsymbol{\beta}}_n\right)\right] \tag{36}$$

where $\tilde{\boldsymbol{\beta}}_n^{\mathrm{T}}\, \tilde{\boldsymbol{\beta}}_n > 0$, therefore V is positive definite. Differentiating Equation (36), considering Equations (14), (16), (17), (18) and after mathematical manipulations, one obtains:

$$\dot{V} = \boldsymbol{\sigma}^{\mathrm{T}}\dot{\boldsymbol{\sigma}} + \sum_{n=1}^{\mathrm{N}} \left(\tilde{\boldsymbol{\beta}}_n^{\mathrm{T}} \dot{\tilde{\boldsymbol{\beta}}}_n\right) = \boldsymbol{\sigma}^{*^{\mathrm{T}}} \boldsymbol{B}_{0\sigma}^{-1} \boldsymbol{A}_{0\sigma} + \boldsymbol{\sigma}^{*^{\mathrm{T}}} \left(\boldsymbol{v} + \tilde{\boldsymbol{d}}_0\right) + \sum_{n=1}^{\mathrm{N}} \tilde{\boldsymbol{\beta}}_n^{\mathrm{T}} \dot{\tilde{\boldsymbol{\beta}}}_n.$$

Using the control law (AFVSC), Equation (30), and replacing Equations (32) and (34), $\dot{V}$ results in:

$$\dot{V} = -\boldsymbol{\sigma}^{*^{\mathrm{T}}}\mathbf{K}\boldsymbol{\sigma}^* + \sum_{n=1}^{\mathrm{N}} \sigma_n^* \left[\tilde{\boldsymbol{d}}_{0_n} - \boldsymbol{\beta}_n^{\mathrm{T}}\boldsymbol{\psi}_n(\sigma_n^*)\right] - \sum_{n=1}^{\mathrm{N}} \sigma_n^* \tilde{\boldsymbol{\beta}}_n^{\mathrm{T}}\boldsymbol{\psi}_n(\sigma_n^*) + \sum_{n=1}^{\mathrm{N}} \tilde{\boldsymbol{\beta}}_n^{\mathrm{T}}\dot{\tilde{\boldsymbol{\beta}}}_n.$$

Replacing the adaptive law Equation (35), $\dot{V}$ yields in:

$$\dot{V} = -\boldsymbol{\sigma}^{*^{\mathrm{T}}}\mathbf{K}\boldsymbol{\sigma}^* + \sum_{n=1}^{\mathrm{N}} \sigma_n^* \left[\tilde{\boldsymbol{d}}_{0_n} - \boldsymbol{\beta}_n^{\mathrm{T}}\boldsymbol{\psi}_n(\sigma_n^*)\right]. \tag{37}$$

From Equation (32), assume that:

$$\left|\tilde{\boldsymbol{d}}_{0_n} - \boldsymbol{\beta}_n^{\mathrm{T}}\boldsymbol{\psi}_n(\sigma_n^*)\right| \leq \gamma_n \leq \phi_n|\sigma_n^*|$$

where $0 < \phi_n < 1$. Then, the second term at the right side of Equation (37) satisfies

$$\sigma_n^* \left|\tilde{\boldsymbol{d}}_{0_n} - \boldsymbol{\beta}_n^{\mathrm{T}}\boldsymbol{\psi}_n(\sigma_n^*)\right| \leq \phi_n|\sigma_n^*|^2 = \phi_n\sigma_n^{*^2}$$

therefore

$$\dot{V} \leq -\boldsymbol{\sigma}^{*^{\mathrm{T}}}\mathbf{K}\boldsymbol{\sigma}^* + \sum_{n=1}^{\mathrm{N}} \phi_n\sigma_n^{*^2}. \tag{38}$$

The right side of Equation (38) can be written as

$$\dot{V} \leq \sum_{n=1}^{\mathrm{N}} \left(-\kappa_n\sigma_n^{*^2} + \phi_i\sigma_n^{*^2}\right) = -\boldsymbol{\sigma}^{*^{\mathrm{T}}}(\mathbf{K} - \boldsymbol{\phi})\boldsymbol{\sigma}^* \leq 0,$$

considering $\mathbf{K} = diag[\kappa_1 \ldots \kappa_n \ldots \kappa_{\mathrm{N}}]$ and $\boldsymbol{\phi} = diag[\phi_1 \ldots \phi_n \ldots \phi_{\mathrm{N}}]$. Simply choose $\kappa_n > \phi_n$ so that $\mathbf{K} - \boldsymbol{\phi}$ is a positive definite matrix, therefore $\dot{V} \leq 0$. Since $\mathbf{K} - \boldsymbol{\phi}$ is a positive definite matrix, $\dot{V} = 0$ only when $\boldsymbol{\sigma}^* = 0$. Thus, the AFVSC is asymptotically stable.

4.4. **Extracting rule base.** To decide the rules for the fuzzy systems, consider V as in Equation (20). V is regarded as an indicator of the energy of $\boldsymbol{\sigma}$. The stability of the system is guaranteed by choosing a control law such that $\dot{V} \leq 0$. In the AFVSC, Equation (30), a fuzzy system $\hat{\boldsymbol{F}}(\boldsymbol{\sigma}^*)$ Equation (31), is applied to compensating the uncertainties and disturbances in the system and to reduce the energy of $\boldsymbol{\sigma}^*$. In this case, $\dot{V}$, Equation (37), can be rewritten as:

$$\dot{V} = \sum_{n=1}^{\mathrm{N}} \left[\sigma_n^* \left(\tilde{d}_{0_n} - \hat{f}_n(\sigma_n^*)\right)\right] - \boldsymbol{\sigma}^{*^{\mathrm{T}}}\mathbf{K}\boldsymbol{\sigma}^*. \tag{39}$$

Because of the function $sign(\boldsymbol{\sigma}^*)$ the control gain has the same signal as $\boldsymbol{\sigma}^*$. Therefore, $\hat{f}_n(\sigma_n^*)$ should have the same signal as σ_n^*. Now consider $\sigma_n^* \left[\tilde{d}_{0_n} - \hat{f}_n(\sigma_n^*)\right]$. When $|\sigma_n^*|$ is large, it is expected that $\left|\hat{f}_n(\sigma_n^*)\right|$ is larger so that $\dot{V}$ has a large negative value. This causes the energy of $\boldsymbol{\sigma}^*$ to decay fast. When $|\sigma_n^*|$ is small, $\sigma_n^* \left[\tilde{d}_{0_n} - \hat{f}_n(\sigma_n^*)\right]$ is also small and has little effect on the value of $\dot{V}$. Then $\left|\hat{f}_n(\sigma_n^*)\right|$ can be small to avoid chattering. When $|\sigma_n^*|$ is zero, $\left|\hat{f}_n(\sigma_n^*)\right|$ is also zero. With this analysis, the rule base is chosen as:

- IF σ_n^* is NB, THEN $\hat{f}_n(\sigma_n^*)$ is $\hat{\beta}_n^{1^{\mathrm{T}}}\psi_n^1(\sigma_n^*)$

- IF σ_n^* is NM, THEN $\hat{f}_n(\sigma_n^*)$ is $\hat{\beta}_n^{2^{\mathrm{T}}}\psi_n^2(\sigma_n^*)$
- IF σ_n^* is NS, THEN $\hat{f}_n(\sigma_n^*)$ is $\hat{\beta}_n^{3^{\mathrm{T}}}\psi_n^3(\sigma_n^*)$
- IF σ_n^* is ZE, THEN $\hat{f}_n(\sigma_n^*)$ is $\hat{\beta}_n^{4^{\mathrm{T}}}\psi_n^4(\sigma_n^*)$
- IF σ_n^* is PS, THEN $\hat{f}_n(\sigma_n^*)$ is $\hat{\beta}_n^{5^{\mathrm{T}}}\psi_n^5(\sigma_n^*)$
- IF σ_n^* is PM, THEN $\hat{f}_n(\sigma_n^*)$ is $\hat{\beta}_n^{6^{\mathrm{T}}}\psi_n^6(\sigma_n^*)$
- IF σ_n^* is PB, THEN $\hat{f}_n(\sigma_n^*)$ is $\hat{\beta}_n^{7^{\mathrm{T}}}\psi_n^7(\sigma_n^*)$

where N stands for negative, P positive, ZE zero, S small, M medium, and B big.

The membership functions are chosen to be triangular-shaped functions as:

$$\mu_n^m(\sigma_n^*) = \begin{cases} 0, & \sigma_n^* \leq \alpha_1 \\ \dfrac{\sigma_n^* - \alpha_1}{\alpha_2 - \alpha_1}, & \alpha_1 \leq \sigma_n^* \leq \alpha_2 \\ \dfrac{\alpha_3 - \sigma_n^*}{\alpha_3 - \alpha_2}, & \alpha_2 \leq \sigma_n^* \leq \alpha_3 \\ 0, & \alpha_3 \leq \sigma_n^* \end{cases} \tag{40}$$

where α_1 and α_3 are the "feet" of the triangle, and the parameter α_2 locates the peak. The parameters of the input membership functions are predefined, and given in Table 1.

TABLE 1. Parameters of the membership functions of σ^*

	σ_1^*			σ_2^*		
	α_1	α_2	α_3	α_1	α_2	α_3
NB	$-\infty$	-0.3	-0.2	$-\infty$	-0.5	-0.33
NM	-0.3	-0.2	-0.1	-0.5	-0.33	-0.16
NS	-0.2	-0.1	0	-0.33	-0.16	0
ZE	-0.1	0	0.1	-0.16	0	0.16
PS	0	0.1	0.2	0	0.16	0.33
PM	0.1	0.2	0.3	0.16	0.33	0.5
PB	0.2	0.3	∞	0.33	0.5	∞

It must be emphasized that the processing time required when using fuzzy logic control depends upon the number of rules that must be evaluated. Moreover, large systems with many rules would require very powerful and fast processors to compute in real-time. The smaller the rule base is, the less computational power it needed [30]. Thus, unlike a pure fuzzy logic controller which is encountered in the rule expanding problem, the AFVSC, as the simplest model, uses only 7 if-then rules in the rule base with respect to sliding surfaces, as well as it uses triangular membership functions, making their structure even simpler and suitable for implementation in real DWMRs. In addition, the reasons to choose this fuzzy inference system with respect to other methods are: to be a simpler model; to control the system efficiently, being best suited for control applications; to be used often due to the intuitive nature of the system and ease in designing. Further details about this choice can be found in [56, 57].

5. **Simulation and Experimental Results.** In order to verify the performance of the controllers described in Sections 3 and 4, the VSC and the AFVSC are implemented in Matlab/Simulink software, version R2014a, and evaluated for the trajectory tracking control problem by means of: simulation using the DWMR model proposed in Section 2;

DWMR simulator – the MobileSim; and application in the PowerBot DWMR. The Matlab/Simulink executions were performed with the Euler integration method with sampling time of 5 ms. Other integration methods were tested, but only with marginal improvement.

The trajectory used as reference trajectory was an eight-shape trajectory [58]. This trajectory is more complex, considering the deceleration and acceleration, with the linear velocity varying between 0.15 m/s and 0.45 m/s and the angular velocity varying between -0.7 rad/s and 0.7 rad/s along the trajectory, as well as it has an initial error $\boldsymbol{q}_{\mathrm{e}} = \left[0.15\ 0.2\ \frac{\pi}{6}\right]^{\mathrm{T}}$. The mathematical formulation of this trajectory is given by Equation (41), and the reference trajectory and velocities are illustrated in Figure 4.

$$\dot{\boldsymbol{q}}_{\mathrm{r}} = \begin{bmatrix} \dot{x}_{\mathrm{r}} \\ \dot{y}_{\mathrm{r}} \\ \dot{\theta}_{\mathrm{r}} \end{bmatrix} = \begin{bmatrix} \frac{3\pi}{50} \sin\left(\frac{2\pi}{50}\left(t + \frac{50}{4}\right)\right) \\ -\frac{6\pi}{50} \cos\left(\frac{4\pi}{50}\left(t + \frac{50}{4}\right)\right) \\ \dfrac{\ddot{y}_{\mathrm{r}}\dot{x}_{\mathrm{r}} - \ddot{x}_{\mathrm{r}}\dot{y}_{\mathrm{r}}}{\dot{x}_{\mathrm{r}}^2 + \dot{y}_{\mathrm{r}}^2} \end{bmatrix}, \quad \boldsymbol{v}_{\mathrm{r}} = \begin{bmatrix} \upsilon_{\mathrm{r}} \\ \omega_{\mathrm{r}} \end{bmatrix} = \begin{bmatrix} \sqrt{\dot{x}_{\mathrm{r}}^2 + \dot{y}_{\mathrm{r}}^2} \\ \dot{\theta}_{\mathrm{r}} \end{bmatrix}. \tag{41}$$

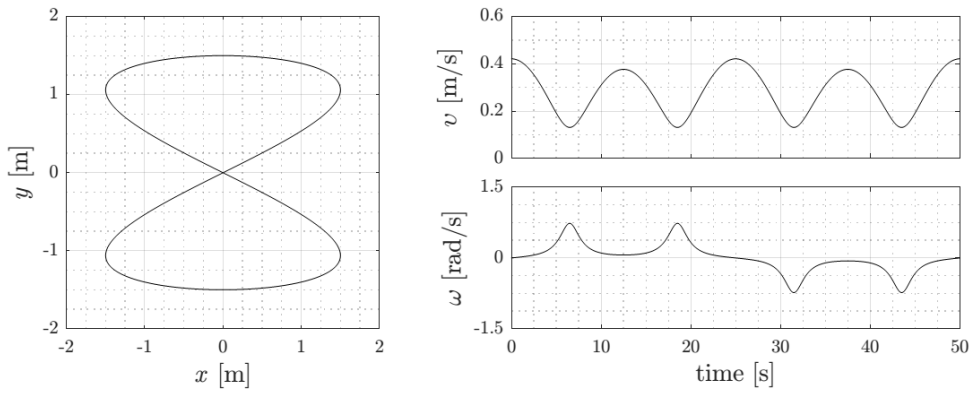

FIGURE 4. Eight-shape reference trajectory and velocities

TABLE 2. Gains of the sliding surfaces for the eight-shape trajectory

Trajectory	**Gain**		
	Λ_1	Λ_2	Λ_3
Eight-shape	1.5	6.0	1.0

The gains of the sliding surfaces for this trajectory and the gains of the kinematic and dynamic controllers are presented in Tables 2 and 3, respectively. Also, with respect to these tables, the gains of the kinematic controllers were obtained through optimization using the design optimization toolbox of Matlab/Simulink, while the gains of the dynamic controller are provided by the manufacturer of PowerBot DWMR. In addition, $\hat{\boldsymbol{\beta}}_n$ parameter of the adaptation law Equation (35), is initialized to zero. Therefore, the gains of these tables were not obtained by trial and error.

Unfortunately, as appointed in Subsection 3.1, the low-control architecture of the PowerBot DWMR is closed and there is an internal PD controller that tracks velocities inputs with a sampling time of 5 ms. Thus, only this internal PD controller can be considered as dynamic controller in all simulated and practical experiments. Actually, this unpleasant situation is commonly found in the literature of robotics as in [50, 52].

TABLE 3. Gains of the kinematic and dynamic controllers

Gain	Controller	
	VSC	AFVSC
g_1	0.1	–
g_2	0.3	–
κ_1	0.1	0.1
κ_2	0.1	0.1
$k_{p\upsilon}$	40.0	40.0
$k_{p\omega}$	40.0	40.0
$k_{d\upsilon}$	20.0	20.0
$k_{d\omega}$	20.0	20.0
η_υ	1.0	1.0
η_ω	1.0	1.0

5.1. **Simulation results in ideal scenario.** In the first simulation scenario, called ideal scenario, the kinematic Equation (1), and dynamic Equation (2), models are considered to represent the PowerBot DWMR, disregarding uncertainties and disturbances (e.g., external disturbances, $\boldsymbol{\delta}(\boldsymbol{q}, \boldsymbol{v}) = 0$). These simulations were made in Matlab/Simulink, following the block diagram presented in Figure 5.

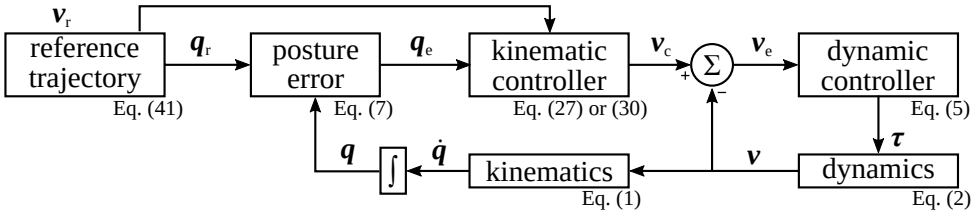

FIGURE 5. Block diagram of simulation or ideal scenario

The results of the VSC and AFVSC simulated in this scenario are presented in Table 4. This table shows the root mean square (RMS) of the errors, being the position errors given by $xy_e = \sqrt{x_e^2 + y_e^2}$ (in meters) and the orientation error given by θ_e (in radians). RMS is an evaluation method commonly used in [49,50,59], and is given by $\text{RMS} = \left[\frac{1}{T}\sum x^2(i)\right]^{\frac{1}{2}}$, where T is the number of samples, and $x(i)$ is the i-th sample.

TABLE 4. RMS of the errors – Simulation results in ideal scenario

Controller	Signal	RMS errors
VSC	xy_e	0.0358 [m]
	θ_e	0.0725 [rad]
AFVSC	xy_e	0.0382 [m]
	θ_e	0.0828 [rad]

These results shown in Table 4 evince that both controllers can track the trajectory with sufficient error performance. Considering the eight-shape trajectory difficulty and its initial error, Figure 6(a) confirms visually the results of Table 4, which presents the DWMR satisfactorily tracing the reference trajectory. Although both controllers lead the DWMR to track the trajectory, in Figure 6(b) it can be seen that the VSC presents lower errors than the AFVSC.

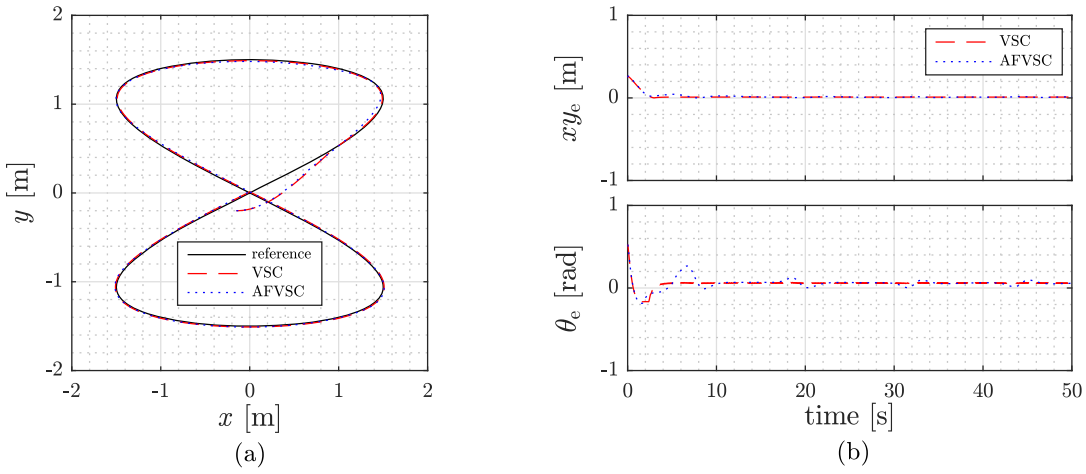

FIGURE 6. Trajectory tracking (a), posture tracking errors (b) in the ideal scenario

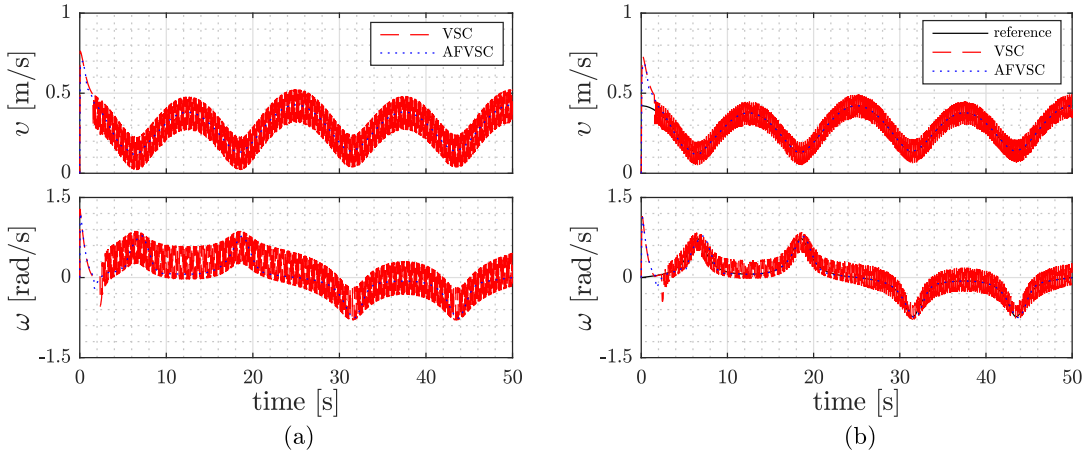

FIGURE 7. Control signals (a) and executed velocities (b) of the DWMR in the ideal scenario

Figure 7(a) shows the linear and angular control velocities of the two controllers. The high chattering can be observed on the control velocities of the VSC, while the continuous approximation of the AFVSC has smooth control velocities and the chattering was eliminated. In Figure 7(b), it can be evinced that for both controllers the executed velocities tend to reference velocities; however, the VSC signals cause chattering in executed velocities while AFVSC do not. Both sliding surfaces (VSC and AFVSC) converge to zero, as can be observed in Figure 8 without chattering phenomenon.

It is known that the kinematic controllers (VSC and AFVSC) contain a function to correct the posture tracking errors, whereas the dynamic controller (PD) aims to correct the auxiliary velocity tracking errors ($\boldsymbol{v}_e$). With these controllers working together, the perfect velocity tracking is not reached. Thus, the auxiliary velocity tracking errors are assumed as disturbances to the kinematic model and are compensated by these kinematic controllers, ensuring that the posture tracking errors tend to zero and yielding satisfactory trajectory tracking performance (Figure 6). This behaviour can be observed in Figure 9, whose auxiliary velocity tracking errors and compensations have opposed magnitudes (aiming cancellation). Moreover, in Figure 9(a) it can be verified of the chattering phenomenon in the compensation due to the use of VSC. Also, it is important to emphasize that, under the robustness considerations treated previously, if a controller is able to compensate the auxiliary velocity tracking errors, then it is a robust controller to

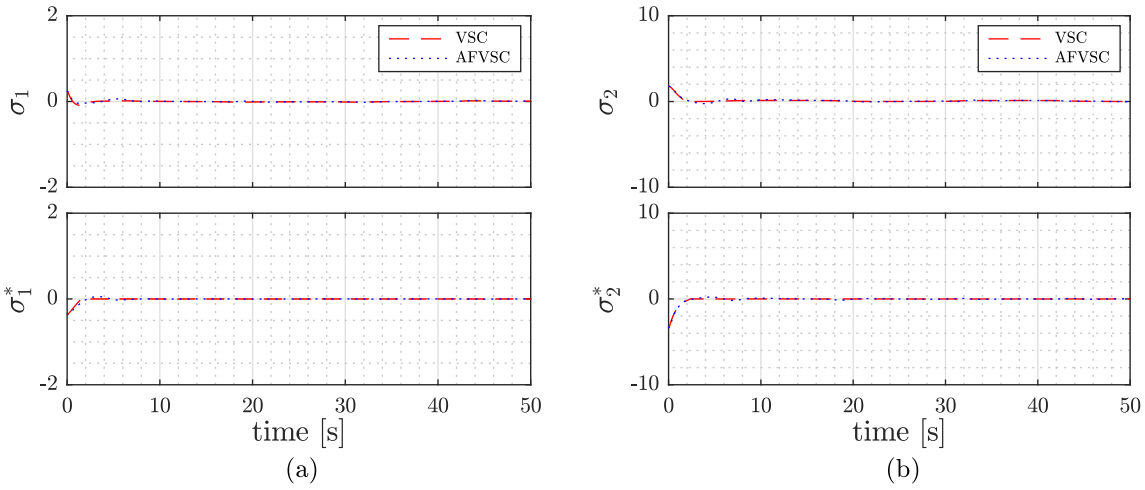

FIGURE 8. Sliding surfaces σ_1, σ_1^* (a) and σ_2, σ_2^* (b) in the ideal scenario

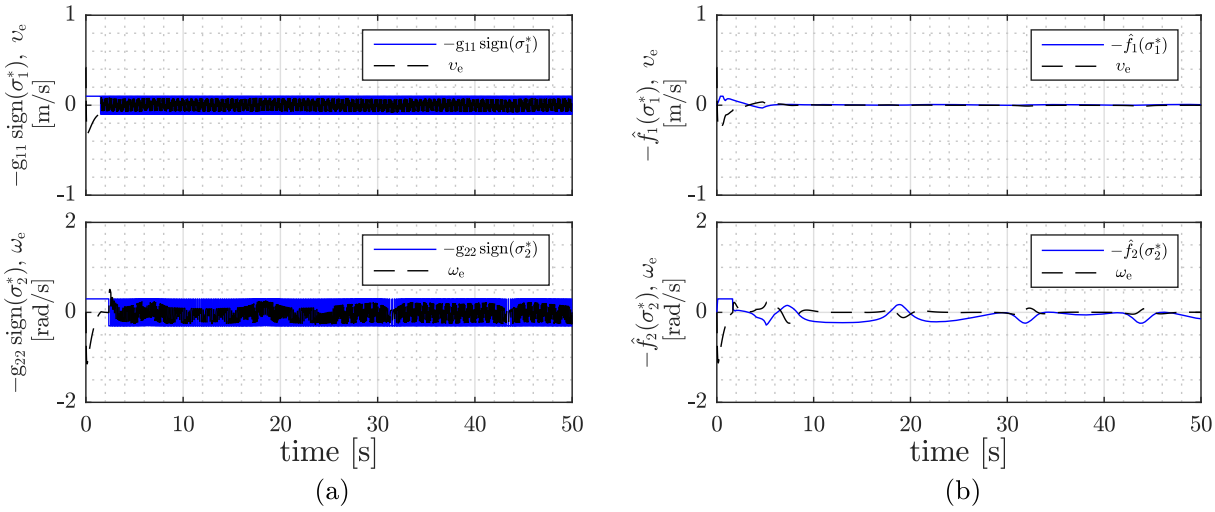

FIGURE 9. Auxiliary velocity tracking errors and compensations using VSC (a) and AFVSC (b) in the ideal scenario

matched uncertainties and disturbances. Thus, the VSC is robust by using discontinuous function $-\mathbf{G}sign(\boldsymbol{\sigma}^*)$. The AFVSC compensates the auxiliary velocity tracking errors by the function $-\hat{\boldsymbol{F}}(\boldsymbol{\sigma}^*)$.

The simulations in the ideal scenario show slightly better tracking results for the VSC at cost of high chattering. This high chattering is considered as a large drawback due to the reduction of the DWMR useful life, while the tracking performance is just slightly better in relation to AFVSC. It is important to recall that in the ideal scenario uncertainties and disturbances (e.g., physical limitations, unmodeled dynamics, modeling imprecision and external disturbances) of the DWMR are not considered, thus the DWMR can reproduce the control velocities with high chattering, which is not true when considering a real DWMR. This is verified ahead in the realistic scenario (MobileSim simulator) and experiments in real-time (PowerBot DWMR).

5.2. **Simulation results in realistic scenario.** This simulation scenario, called the realistic scenario, instead of using the models developed in Section 2 to represent the DWMR used the MobileSim simulator. This software is designed to simulate the behavior

of robotic platforms produced by Omron Adept MobileRobots Inc. aiming at debugging and experimentation.

To establish communication between the controller (Matlab/Simulink) and the MobileSim simulator the ARIA (Advanced Robot Interface for Applications) library is used. This library implements functions to manipulate the velocity, heading, relative heading and other motion parameters of the DWMRs. ARIA also receives position estimation, sonar readings, and all other current operating data sent by the robotic platform.

The block diagram presented in Figure 10 shows how ARIA and MobileSim simulator were used to make the simulations in the realistic scenario.

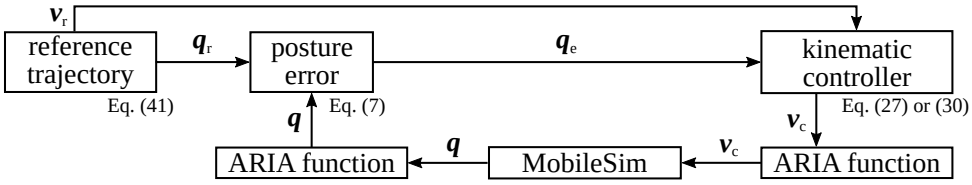

FIGURE 10. Block diagram of the simulations in the realistic scenario

As in the ideal scenario, the VSC and AFVSC were simulated in the realistic scenario for the eight-shape trajectory, whose results of the trajectory tracking, control velocities, executed velocities, sliding surfaces, auxiliary velocity tracking errors and compensations of the VSC and AFVSC, are presented graphically in the sequence. Also, it is emphasized that MobileSim simulator considers the uncertainties and disturbances (e.g., parametric variations, unmodeled dynamics and physical limitations) of the DWMR.

The results in Table 5, containing RMS of the errors, show that the two controllers can track the trajectory with sufficient error performance even with uncertainties and disturbances.

TABLE 5. RMS of the errors – Simulation results in the realistic scenario using MobileSim simulator

Controller	**Signal**	**RMS errors**
VSC	xy_e	0.1299 [m]
	θ_e	0.1335 [rad]
AFVSC	xy_e	0.1252 [m]
	θ_e	0.0940 [rad]

The reference trajectory, with respect to realized trajectory by the DWMR using the two controllers, is illustrated in Figure 11(a). From this figure, it can be verified that the DWMR gets to the trajectory at a similar point and remains near the trajectory during the remaining time, i.e., the DWMR tracks the reference trajectory.

Figure 11(b) shows the posture tracking errors, where the VSC varies more slightly than the AFVSC. This variation, with more intensity in the orientation error, means that the DWMR executes a displacement with a zigzag around the desired trajectory. For the AFVSC, the errors tend to zero with a slight variation at orientation error when the DWMR makes a curve, showing the difficulty of the eight-shape trajectory at the points of high variation in values of reference velocities.

In Figure 12(a), the control velocities are shown where the VSC presents a large chattering, both in linear and angular velocities, while the AFVSC shows smooth control signals. These same behaviors can also be observed in Figure 12(b) in which velocities of the DWMR track the reference velocities.

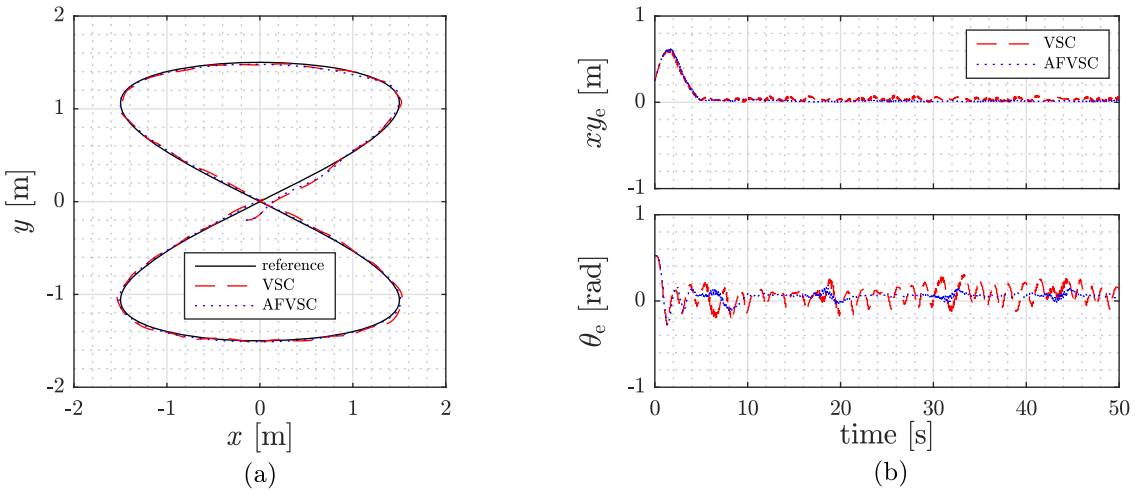

FIGURE 11. Trajectory tracking (a), posture tracking errors (b) in the realistic scenario

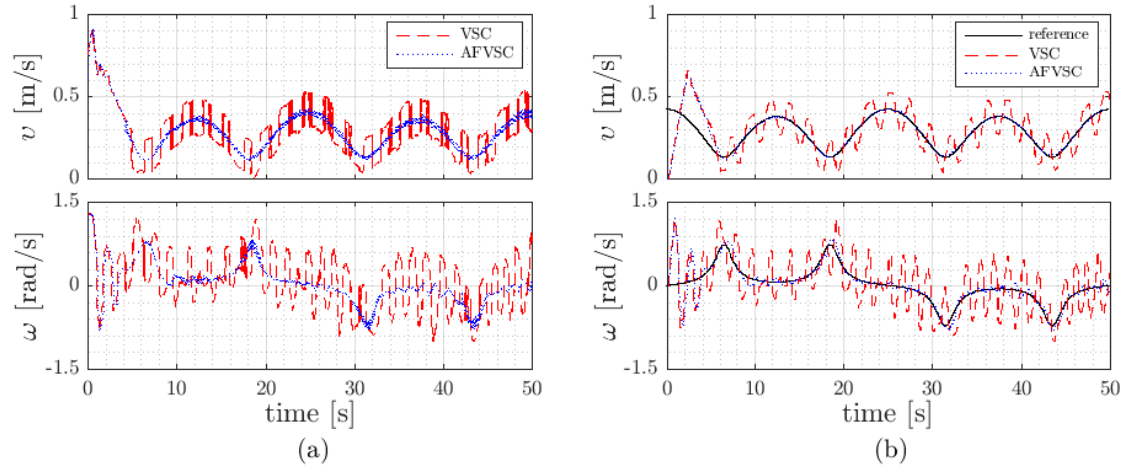

FIGURE 12. Control velocities (a) and velocities of the DWMR (b) in the realistic scenario

For the use of the AFVSC, the sliding surfaces tend to converge to zero, as can be seen in Figure 13 without chattering phenomenon, while for the use of VSC these sliding surfaces present behaviors alternating near zero.

The auxiliary velocity tracking errors $\boldsymbol{v}_e$, seen as disturbances for the kinematic model, happen because of uncertainties and disturbances. Figure 14 shows the auxiliary velocity tracking errors and compensations for the use of the two controllers.

Unlike the ideal scenario, in this scenario Figure 12 shows how the DWMR cannot switch instantaneously the control velocities and the velocities of the DWMR, generating large auxiliary velocity tracking errors. As a consequence, the compensations do not generate the control efforts with equal or higher magnitudes than the auxiliary velocity tracking errors, as can be seen in Figure 14(a), by using the VSC. In addition, the AFVSC in Figure 14(b) presents auxiliary velocity tracking errors and compensations, whose magnitudes have opposed behaviors in absolute terms with the aim of cancelling.

The results show a slightly better tracking performance of the AFVSC when compared to the VSC, recalling that the VSC, as drawbacks, presents high chattering, and requires *a priori* the knowledge of the limits of the uncertainties and disturbances to define the

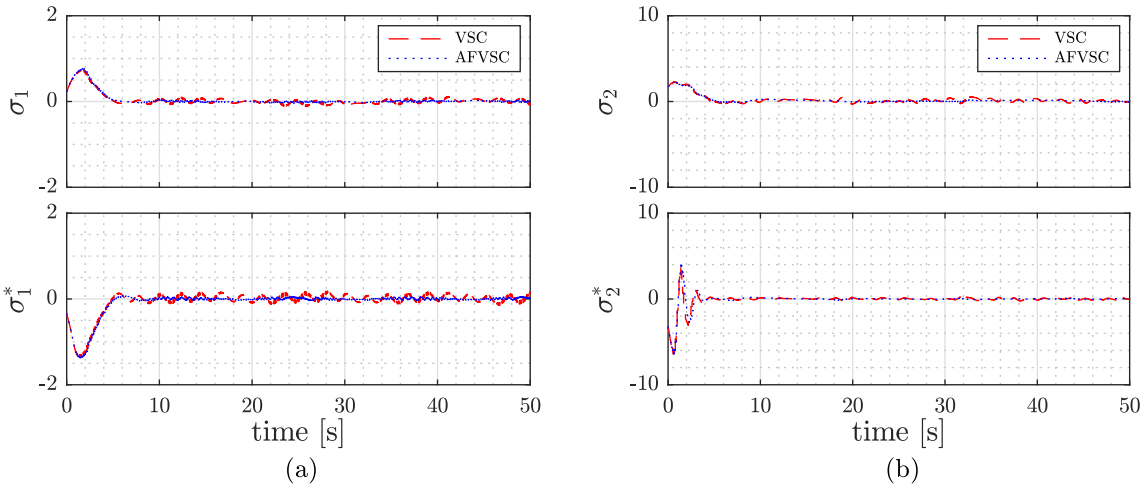

FIGURE 13. Sliding surfaces σ_1, σ_1^* (a) and σ_2, σ_2^* (b) in the realistic scenario

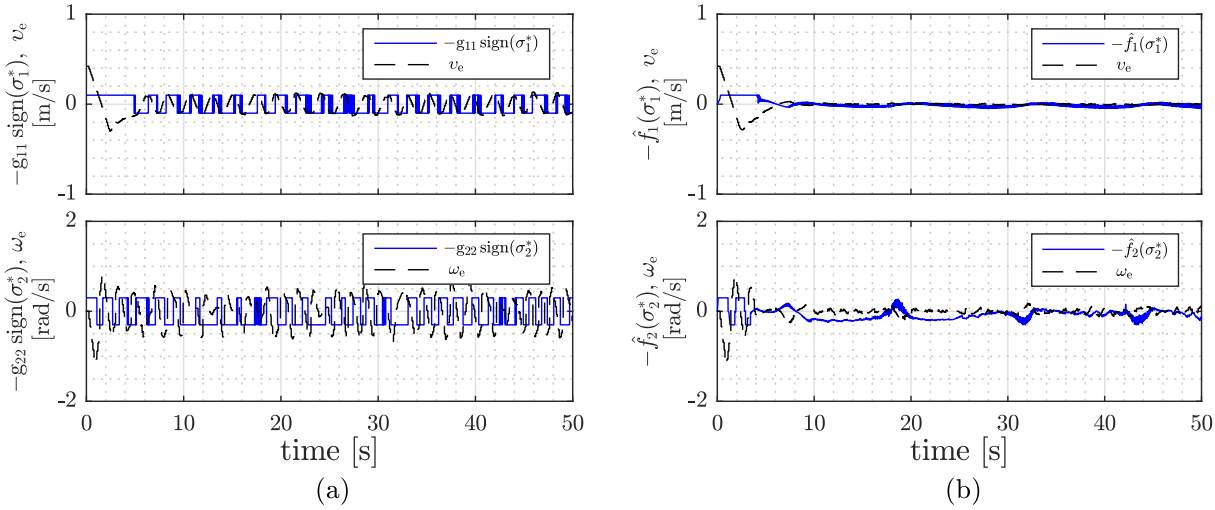

FIGURE 14. Auxiliary velocity tracking errors and compensations using VSC (a) and AFVSC (b) in the realistic scenario

gain values matrix $\mathbf{G}$, to achieve a satisfactory tracking performance, resulting in unnecessary control efforts to the actuators of the DWMR. Moreover, the difference in the tracking results from the ideal scenario to the realistic scenario is due to uncertainties and disturbances (e.g., physical limitations, unmodeled dynamics and external disturbances) of the DWMR.

5.3. **Real DWMR implementation.** In this scenario the proposed controller is tested in the PowerBot DWMR, a high-payload differential drive robotic platform for research and rapid prototyping. It is a platform for laboratory and research tasks involving delivery, navigation and handling of large payloads. PowerBot DWMR is a member of MobileRobots Pioneer family of mobile robots, which are research and development platforms that share a common architecture, foundation software and employ intelligence based client-server robotic control [46]. Table 6 shows the parameters of the PowerBot DWMR.

Figure 15 shows the block diagram of the execution where the simulator MobileSim of Figure 10 was replaced by the PowerBot DWMR. ARIA is still used for the comunication (serial RS-232 port) between the Matlab/Simulink and the PowerBot DWMR.

TABLE 6. Parameter specifications of the PowerBot DWMR

Parameter	Value	Parameter	Value
Body mass	120 kg	Max. payload	100 kg
Drive wheel radius	0.135 m	Moment of inertia	15.0656 kg.m^2
DWMR height	0.48 m	Max. linear velocity	2.1 m/s
DWMR length	0.9 m	Max. angular velocity	$\frac{5\pi}{3}$ rad/s $\approx$ 5.24 rad/s
DWMR width	0.66 m	Max. motor torque	20.45 Nm

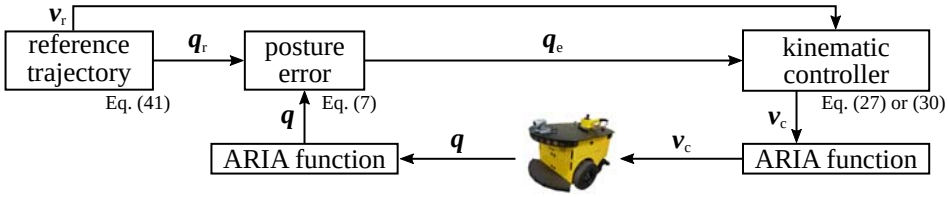

FIGURE 15. Block diagram of real DWMR implementation or experimental scenario

TABLE 7. RMS of the errors – Experimental results

Controller	Signal	RMS errors
AFVSC	xy_e	0.0892 [m]
	θ_e	0.1176 [rad]

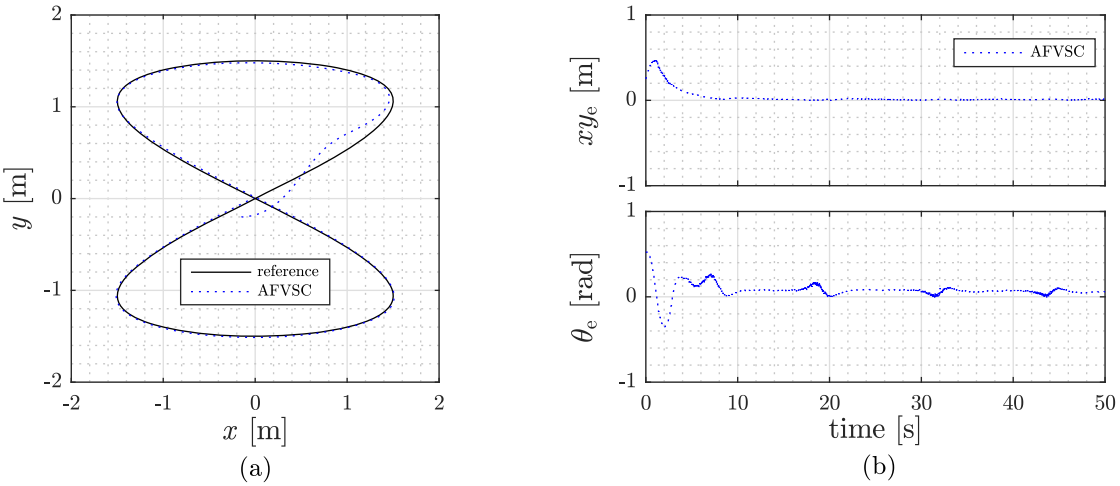

FIGURE 16. Trajectory tracking (a) and posture tracking errors (b) in the experimental scenario

For this scenario the AFVSC was tested in the PowerBot DWMR for the eight-shape trajectory. Table 7 presents the RMS of the errors for this experimentation. It must be emphasized that the practical implementation of VSC was not carried out in the PowerBot DWMR for determining the chattering phenomenon, which causes performance degradation, as well as to verify the occurrence of impossibility of the ideal switching in high frequency required by the control signal, because the switching in high frequency causes reduction in the useful life of the actuators as well as to prevent further damage to PowerBot DWMR.

The experimental results in real-time, presented in Table 7, confirm what was observed in the simulation results, AFVSC can track the trajectory with sufficient error performance. Figures 16 to 19 show graphically the experimental results of the AFVSC on the

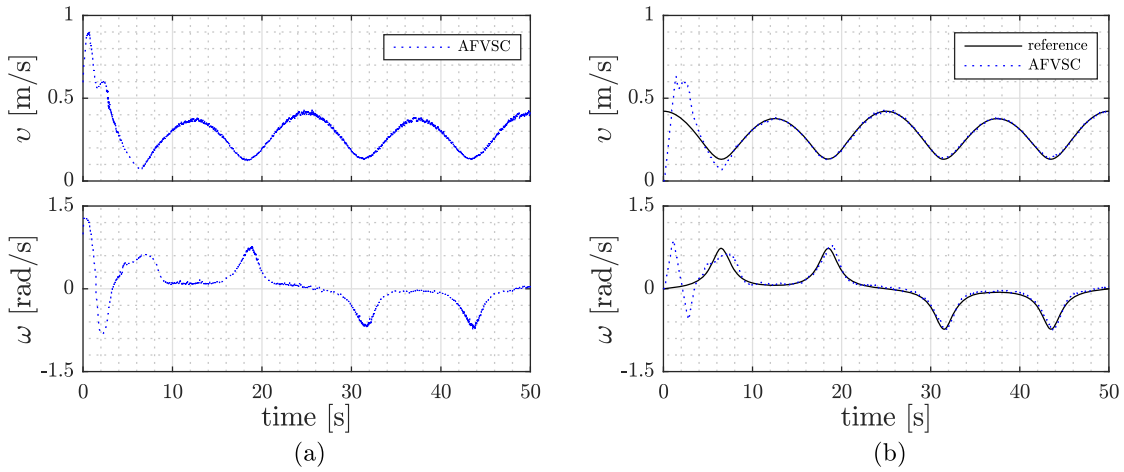

FIGURE 17. Control velocities (a) and velocities (b) of the DWMR in the experimental scenario

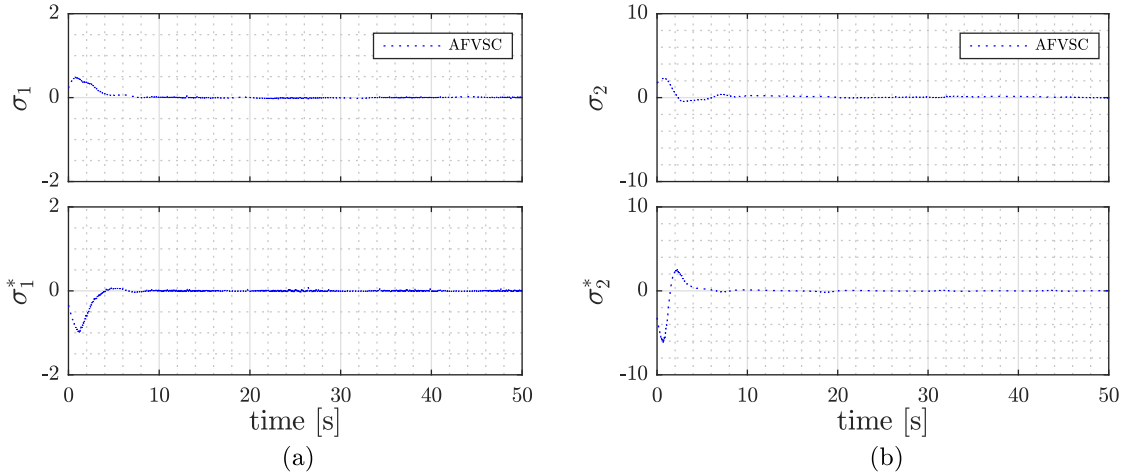

FIGURE 18. Sliding surfaces σ_1, σ_1^* (a) and σ_2, σ_2^* (b) in the experimental scenario

PowerBot DWMR. Figure 16(a) shows how the DWMR reaches the reference trajectory, and remains on it during the entire experiment. In Figure 16(b), it is observed how the posture tracking errors tend to zero and has a behavior similar to that obtained in MobileSim simulator (realistic scenario).

The control velocities generated by the AFVSC have smooth control signals, as illustrated in Figure 17(a). With respect to the velocities of DWMR, it can be observed in Figure 17(b) that they track the reference velocities.

From the observation of Figure 18, it can be verified that the sliding surfaces tend to zero and are free from chattering.

Figure 19 shows how the AFVSC is robust to matched uncertainties and disturbances, whose behaviors of auxiliary velocity tracking errors and compensations are similar to behaviors obtained using the MobileSim simulator (realistic scenario).

In short, the results in the experimental scenario are coherent with the results obtained in the realistic scenario. Based on the experimental results, it is verified that Remark 2.1 provided in [48], i.e., the realization of the invariance requires that switching between the reaching phase and the sliding phase is ideal, is impractical. Therefore, the invariance is ideal and has little practical meaning.

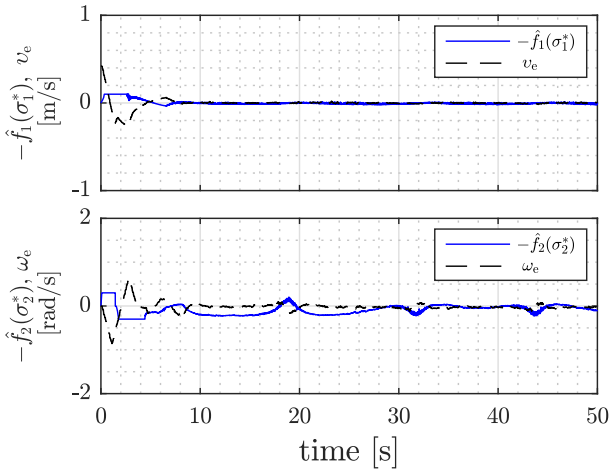

FIGURE 19. Auxiliary velocity tracking errors and compensations using AFVSC in the experimental scenario

6. **Conclusions.** In this paper, the integration of a kinematic controller (AFVSC) and a dynamic controller (PD control) as a solution to the trajectory tracking problem applied to DWMRs was proposed. For purposes of performance comparison with the AFVSC, a VSC, as a kinematic controller, was also integrated to the PD controller. Sufficient analysis results were obtained studying the two kinematic controllers over the same PD controller.

The AFVSC was obtained from VSC, and the VSC was considered because of its ability to apply the invariance principle and its drawback on exhibiting the chattering phenomenon (which is highly undesirable). To avoid the chattering phenomenon, as well as to suppress the uncertainties and disturbances, an adaptive fuzzy inference system was used in the replacement of the discontinuous portion of the classical VSC. Due to the replacement, the invariance principle was not verified anymore; however, the robustness is ensured and a smooth control signal is achieved.

The results obtained in MobileSim simulator (realistic scenario) and in the implementation over the PowerBot DWMR (experimental scenario) have shown that the AFVSC has better performance than the VSC, indicating that the invariance has little pratical meaning.

It must be emphasized that the advantage of the AFVSC in comparison to the VSC, appears also in two other characteristics: the online update of the output parameters of the fuzzy system, which remove the need of *a priori* knowledge of the limits of uncertainties and disturbances in the system; and no need of application of a large value to the gains $\mathbf{G}$ that can cause high control efforts unnecessary to DWMR actuators, reducing its useful life.

In fact, the integration of the AFVSC controller with the PD controller demonstrated that the incidence of uncertainties and disturbances produces auxiliary velocity tracking errors. These auxiliary velocity tracking errors did not converge to zero; therefore, the PD controller did not consider the uncertainties and disturbances, and the control efforts produced by this controller were not sufficient to compensate for them. Indeed, these auxiliary velocity tracking errors were viewed as uncertainties and disturbances for the kinematic model, and the AFVSC controller contained the function to compensate such tracking errors, thus driving the convergence of the posture tracking errors to zero and supplying significant robustness in the reference trajectory tracking without penalizing the control efforts.

Moreover, unlike a pure fuzzy logic controller, the used fuzzy system, as the simplest model with respect to sliding surfaces, uses only 7 if-then rules in the rule base as well as it uses triangular membership functions, making their structure even simpler. Therefore, it has a lower computational load for execution as well as it is more suitable for implementation in real wheeled mobile robots when compared to the related studies in the literature.

The stability analysis of the closed-loop control system with the adaptation law of the fuzzy system, was proved using Lyapunov theory.

In future work, the comparison of AFVSC to other existing chattering reduction approaches (incluing other fuzzy controllers), as well as considering dynamic limitations to generate feasible trajectories to achieve better performance should be made. Another work in progress regards the use of AFVSC in the formation control of DWMRs. Also, some hardware updated for PowerBot DWMR is scheduled, to allow the implementation of direct torque control of the actuators, removing the low-level PD.

Acknowledgements. The authors would like to thank CAPES for the financial support.

REFERENCES

[1] Z. P. Wang, C.-Y. Su, T. H. Lee and S. S. Ge, Robust adaptive control of a wheeled mobile robot violating the pure nonholonomic constraint, *Proc. of the 8th International Conference on Control, Automation, Robotics and Vision*, vol.2, pp.987-992, 2004.

[2] Z. P. Wang, S. S. Ge and T. H. Lee, Adaptive neural network control of a wheeled mobile robot violating the pure nonholonomic constraint, *Proc. of the 43rd IEEE Conference on Decision and Control*, vol.5, pp.5198-5203, 2004.

[3] G. Oriolo, Wheeled robots, *Encyclopedia of Systems and Control*, pp.1-9, 2014.

[4] G. Campion and W. Chung, Wheeled robots, *Springer Handbook of Robotics*, pp.391-410, 2008.

[5] G. Campion, G. Bastin and B. D'Andréa-Novel, Structural properties and classification on kinematic and dynamic models of wheeled mobile robots, *Nelineinaya Dinamika (Russian Journal of Nonlinear Dynamics)*, vol.7, no.4, pp.733-769, 2011.

[6] B. Siciliano and O. Khatib, *Springer Handbook of Robotics*, Springer Science & Business Media, 2008.

[7] J. Y. Hung, W. Gao and J. C. Hung, Variable structure control: A survey, *IEEE Trans. Industrial Electronics*, vol.40, no.1, pp.2-22, 1993.

[8] W. Gao and J. C. Hung, Variable structure control of nonlinear systems: A new approach, *IEEE Trans. Industrial Electronics*, vol.40, no.1, pp.45-55, 1993.

[9] R. A. DeCarlo, S. H. Zak and S. V. Drakunov, Variable structure, sliding mode controller design, *The Control Handbook*, vol.57, pp.941-951, 1996.

[10] V. I. Utkin, J. Guldner and J. Shi, *Sliding Mode Control in Electromechanical Systems*, CRC Press, 2009.

[11] S. Pan, H. Su, X. Hu and J. Chu, Variable structure control theory and application: A survey, *Proc. of the 3rd World Congress on Intelligent Control and Automation*, vol.4, pp.2977-2981, 2000.

[12] O. Kaynak, K. Erbatur and M. Ertugnr, The fusion of computationally intelligent methodologies and sliding mode control – A survey, *IEEE Trans. Industrial Electronics*, vol.48, no.1, pp.4-17, 2001.

[13] H. Lee and V. I. Utkin, Chattering suppression methods in sliding mode control systems, *Annual Reviews in Control*, vol.31, no.2, pp.179-188, 2007.

[14] X. Yu and O. Kaynak, Sliding mode control with soft computing: A survey, *IEEE Trans. Industrial Electronics*, vol.56, no.9, pp.3275-3285, 2009.

[15] M. O. Efe, O. Kaynak and B. M. Wilamowski, Stable training of computationally intelligent systems by using variable structure systems technique, *IEEE Trans. Industrial Electronics*, vol.47, no.2, pp.487-496, 2000.

[16] M. O. Efe and O. Kaynak, Variable structure systems theory based training strategies for computationally intelligent systems, *Proc. of the 27th Annual Conference of the IEEE Industrial Electronics Society*, vol.3, pp.1563-1576, 2001.

[17] Y. Guo and P.-Y. Woo, An adaptive fuzzy sliding mode controller for robotic manipulators, *IEEE Trans. Systems, Man and Cybernetics, Part A: Systems and Humans*, vol.33, no.2, pp.149-159, 2003.

[18] L.-X. Wang, *A Course in Fuzzy Systems and Control*, Prentice-Hall Press, Englewood Cliffs, USA, 1999.

[19] Y. Koubaa, M. Boukattaya and T. Dammak, Adaptive sliding-mode dynamic control for path tracking of nonholonomic wheeled mobile robot, *Journal of Automation and Systems Engineering*, vol.9, no.2, pp.119-131, 2015.

[20] M. Cui, W. Liu, H. Liu, H. Jiang and Z. Wang, Extended state observer-based adaptive sliding mode control of differential-driving mobile robot with uncertainties, *Nonlinear Dynamics*, vol.83, no.1, pp.667-683, 2016.

[21] J. Keighobadi and Y. Mohamadi, Fuzzy sliding mode control of nonholonomic wheeled mobile robot, *Proc. of the 2011 IEEE 9th International Symposium on Applied Machine Intelligence and Informatics*, pp.273-278, 2011.

[22] C. Chen, T. S. Li and Y. Yeh, EP-based kinematic control and adaptive fuzzy sliding-mode dynamic control for wheeled mobile robots, *Information Sciences*, vol.179, nos.1-2, pp.180-195, 2009.

[23] J. Keighobadi and Y. Mohamadi, *Fuzzy Robust Trajectory Tracking Control of WMRs*, Springer US, Boston, MA, 2012.

[24] E. Ozkop, I. H. Altas, H. I. Okumus and A. M. Sharaf, A fuzzy logic sliding mode controlled electronic differential for a direct wheel drive EV, *International Journal of Electronics*, vol.102, no.11, pp.1919-1942, 2015.

[25] A. Mohagheghi, F. Shabaninia and M. Salimifard, Fuzzy logic amp; fuzzy sliding mode tracking control of non-holonomic unicycle wheeled mobile robots, *The 21st Iranian Conference on Electrical Engineering*, pp.1-6, 2013.

[26] R. Bohlouli, Y. Mohamadi, R. Barmaki and J. Keighobadi, Adaptive fuzzy sliding mode controller for wheeled mobile robots, *2011 IEEE Conference on Automation Science and Engineering*, pp.285-290, 2011.

[27] M.-J. Xie, L.-T. Li and Z.-Q. Wang, Robust adaptive control of a wheeled mobile robot violating the pure nonholonomic constraint, *Proc. of the 10th World Congress on Intelligent Control and Automation*, pp.2706-2709, 2012.

[28] J. Keighobadi and Y. Mohamadi, Fuzzy sliding mode control of a nonholonomic wheeled mobile robot, *Proc. of the 2011 International MultiConference of Engineers and Computer Scientists*, vol.2, pp.1-6, 2011.

[29] J. Keighobadi and M. B. Menhaj, From nonlinear to fuzzy approaches in trajectory tracking control of wheeled mobile robots, *Asian Journal of Control*, vol.14, no.4, pp.960-973, 2012.

[30] E. A. Mishra, Trajectory tracking of differential drive wheeled mobile robot, *International Journal on Mechanical Engineering and Robotics*, vol.2, no.2, pp.28-31, 2014.

[31] J. Guldner and V. I. Utkin, Stabilization of nonholonomic mobile robots using Lyapunov functions for navigation and sliding mode control, *Proc. of the 33rd IEEE Conference on Decision and Control*, vol.3, pp.2967-2972, 1994.

[32] H.-S. Shim, J.-H. Kim and K. Koh, Variable structure control of nonholonomic wheeled mobile robot, *Proc. of the 1995 IEEE International Conference on Robotics and Automation*, vol.2, pp.1694-1699, 1995.

[33] J.-M. Yang and J.-H. Kim, Sliding mode control for trajectory tracking of nonholonomic wheeled mobile robots, *IEEE Trans. Robotics and Automation*, vol.15, no.3, pp.578-587, 1999.

[34] J.-M. Yang and J.-H. Kim, Sliding mode motion control of nonholonomic mobile robots, *IEEE Control Systems Magazine*, vol.19, no.2, pp.15-23, 1999.

[35] D. Chwa, J. H. Seo, P. Kim and J. Y. Choi, Sliding mode tracking control of nonholonomic wheeled mobile robots, *Proc. of the 2002 American Control Conference*, vol.5, pp.3991-3996, 2002.

[36] M. Defoort, J. Palos, T. Floquet, A. Kokosy and W. Perruquetti, Practical stabilization and tracking of a wheeled mobile robot with integral sliding mode controller, *Proc. of the 46th IEEE Conference on Decision and Control*, pp.1999-2004, 2007.

[37] M. Defoort, J. Palos, A. Kokosy, T. Floquet and W. Perruquetti, Performance based reactive navigation for nonholonomic mobile robots, *Robotica*, vol.27, no.2, pp.281-290, 2009.

[38] K. Li, X. Wang, M. Yuan, X. Li and S. Wang, Adaptive sliding mode trajectory tracking control of mobile robot with parameter uncertainties, *Proc. of the 2009 IEEE International Symposium on Computational Intelligence in Robotics and Automation*, pp.148-152, 2009.

[39] R. Solea and D. Cernega, Sliding mode control for trajectory tracking problem – Performance evaluation, *Proc. of the 19th International Conference on Artificial Neural Networks*, pp.865-874, 2009.

[40] R. Solea, A. Filipescu and U. Nunes, Sliding mode control for trajectory tracking of a wheeled mobile robot in presence of uncertainties, *Proc. of the 7th Asian Control Conference*, pp.1701-1706, 2009.

[41] J. H. Lee, C. Lin, H. Lim and J. M. Lee, Sliding mode control for trajectory tracking of mobile robot in the RFID sensor space, *International Journal of Control, Automation and Systems*, vol.7, no.3, pp.429-435, 2009.

[42] Y. Li, L. Zhu, Z. Wang and T. Liu, Trajectory tracking for nonholonomic wheeled mobile robots based on an improved sliding mode control method, *International Colloquium on Computing, Communication, Control, and Management*, vol.2, pp.55-58, 2009.

[43] E. S. Elyoussef, N. A. Martins, D. W. Bertol, E. R. De Pieri and M. Jungers, On a wheeled mobile robot trajectory tracking control: 1st and 2nd order sliding modes applied to a compensated inverse dynamics, *Proc. of the 11th Pan-American Congress of Applied Mechanics*, vol.1, pp.1-6, 2010.

[44] N. A. Martins, E. S. Elyoussef, D. W. Bertol, E. R. De Pieri, U. F. Moreno and E. B. Castelan, Nonholonomic mobile robot with kinematic disturbances in the trajectory tracking: A variable structure controller, *Learning and Nonlinear Models*, vol.8, no.1, pp.23-40, 2010.

[45] Y. Liu, Y. Zhang and H. Wang, Tracking control of wheeled mobile robots based on sliding mode control, *Proc. of the 2nd International Conference on Artificial Intelligence, Management Science and Electronic Commerce*, pp.1787-1790, 2011.

[46] A. Filipescu, V. Minzu, B. Dumitrascu and E. Minca, Trajectory tracking and discrete-time sliding-mode control of wheeled mobile robots, *Proc. of the 2011 IEEE International Conference on Information and Automation*, pp.27-32, 2011.

[47] N. A. Martins, M. de Alencar, W. C. Lombardi, D. W. Bertol, E. R. De Pieri and H. Ferasoli Filho, Trajectory tracking of a wheeled mobile robot with uncertainties and disturbances: Proposed adaptive neural control, *Control and Cybernetics*, vol.44, no.1, pp.47-98, 2015.

[48] S. Wang and W. Gao, Robustness and invariance of variable structure systems with multiple inputs, *Proc. of the American Control Conference*, vol.1, pp.1035-1039, 1995.

[49] B. S. Park, S. J. Yoo, J. B. Park and Y. H. Choi, Adaptive neural sliding mode control of nonholonomic wheeled mobile robots with model uncertainty, *IEEE Trans. Control Systems Technology*, vol.17, no.1, pp.207-214, 2009.

[50] E. S. Elyoussef, N. A. Martins, E. R. De Pieri and U. F. Moreno, Pd-super-twisting second order sliding mode tracking control for a nonholonomic wheeled mobile robot, *Proc. of the 19th World Congress of the International Federation of Automatic Control (IFAC World Congress)*, vol.11, pp.3827-3832, 2014.

[51] R. Fierro and F. L. Lewis, Control of a nonholonomic mobile robot using neural networks, *IEEE Trans. Neural Networks*, vol.9, no.4, pp.589-600, 1998.

[52] M. W. Spong, S. Hutchinson and M. Vidyasagar, *Robot Modeling and Control*, Wiley New York, 2006.

[53] Y. Kanayama, Y. Kimura, F. Miyazaki and T. Noguchi, A stable tracking control method for a non-holonomic mobile robot, *Proc. of the IEEE/RSJ International Workshop on Intelligent Robots and Systems*, pp.1236-1241, 1991.

[54] R. A. DeCarlo, S. H. Zak and G. P. Matthews, Variable structure control of nonlinear multivariable systems: A tutorial, *Proc. of the IEEE*, vol.76, no.3, pp.212-232, 1988.

[55] Y. Li, S. Qiang, X. Zhuang and O. Kaynak, Robust and adaptive backstepping control for nonlinear systems using rbf neural networks, *IEEE Trans. Neural Networks*, vol.15, no.3, pp.693-701, 2004.

[56] S. R. Chaudhari and M. E. Patil, Study and review of fuzzy inference systems for decision making and control, *American International Journal of Research Science, Technology, Engineeringand Mathematics*, vol.5, pp.88-92, 2014.

[57] S. R. Chaudhari and M. E. Patil, Comparative analysis of fuzzy inference systems for air conditioner, *International Journal of Advanced Computer Research*, vol.4, no.4, pp.922-927, 2014.

[58] G. Oriolo, A. De Luca and M. Vendittelli, WMR control via dynamic feedback linearization: Design, implementation, and experimental validation, *IEEE Trans. Control Systems Technology*, vol.10, no.6, pp.835-852, 2002.

[59] D. Chwa, Sliding mode tracking control of nonholonomic wheeled mobile robots in polar coordinates, *IEEE Trans. Control Systems Technology*, vol.12, no.4, pp.637-644, 2004.